IDENTIFICATION AND CHARACTERIZATION OF THE INTERACTING PARTNERS AND PHOSPHORYLATION SITES OF EQUILIBRATIVE NUCLEOSIDE TRANSPORTER 1 (ENT1)

BY

PEDRAM MEHRABI

A THESIS SUBMITTED TO THE FACULTY OF GRADUATE STUDIES

IN PARTIAL FULFILMENT OF THE REQUIREMENTS

FOR THE DEGREE OF

MASTER OF SCIENCE

GRADUATE PROGRAM IN BIOLOGY

YORK UNIVERSITY,

TORONTO ONTARIO

OCTOBER 2011

Library and Archives Canada

Published Heritage Branch

395 Wellington Street
Ottawa ON K1A 0N4
Canada

Bibliothèque et Archives Canada

Direction du Patrimoine de l'édition

395, rue Wellington
Ottawa ON K1A 0N4
Canada

Your file Votre référence
ISBN: 978-0-494-91786-2

Our file Notre référence
ISBN: 978-0-494-91786-2

Abstract

Human equilibrative nucleoside transporter 1 (hENT1) is a nucleoside transporter that is a member of the human SLC29 family of integral membrane proteins. Currently nothing is known about proteins that act as interacting partners of ENT1. To identify interactors and gain insight into novel protein-protein interactions (PPIs), membrane yeast two hybrid (MYTH) screening of murine ENT1 with an 11-day whole mouse embryo NubG-X cDNA library was used. Six interacting partners were confirmed with bait dependency tests for murine ENT1. One of these putative interacting partners, calmodulin, was confirmed to interact with hENT1 using NMR spectroscopy and binding affinity was measured using fluorescence anisotropy. The large intracellular loops of human and murine ENT1 were analyzed for potential phosphorylation sites using PKA and LC-MRM mass spectrometry. Both protein constructs showed evidence of specific phosphorylation sites in the large intracellular loop between transmembrane domains 6 and 7. While phosphorylation of ENT1 is known, these are the first data to show which specific residues within the loop are phosphorylated. This systematic analysis of ENT1 confirmed the first interacting partner for hENT1 as well as provided evidence for the location of the phosphosites *in vitro*.

Acknowledgements

The work performed in this thesis has been a culmination of the help of many. It is a pleasure to thank the people that made this thesis possible.

First and foremost, I would like to express my sincere gratitude to my MSc supervisor Prof. Imogen Coe for without your knowledge, patience, and support during my MSc research I would have been completely lost and dumbfounded. Her guidance allowed me to look past the difficulties that come with membrane proteins and to see their beauty.

I would also like to thank my committee member, Prof. Logan Donaldson for your encouragement and insightful comments. Thank you for making me an honorary lab member of your group as well as introducing me to the wonderful world of structural biology.

I am grateful to Prof. Igor Stagljar at the University of Toronto for introducing me to the wonderful world of biochemistry and for the summer internship opportunities throughout the years. Without the opportunities you have given me I would not have gone into graduate school.

I wish to thank Dr. Leroi DeSouza for your help with Mass Spectroscopy; I would still be lost in the data without your help.

I am thankful to many of my colleagues who supported me these past 2 years, Shokoofeh Shahangian, Ekaterina Smirnova, Linda Villani, Dr. German Reyes, Dr. Nicole Nivillac, and especially Dr. Jamie Kwan for the fun discussions, and for making the basement of Farquharson an enjoyable environment to work in. In particular, I am especially grateful to Dr. Jamie Snider, without his endless patience, comraderie, and willingness to put in the time to help me when bombarded with an infinite stream of questions I would not be where I am today.

Last but not least, I would like to thank my parents, Fariba Bozorg and Saeid Mehrabi. Throughout my work and life their love and support has been without limit. To them I dedicate this Thesis.

Table of Contents

List of Tables

List of Figures

List of Abbreviations

3-AT	3-aminotriazole
5-FU	Fluorouracil
ABCA1	ATP-binding Cassette Transporter A1
ACV	Acyclovir
AKT	Protein Kinase B
AMPK	AMP-dependent protein kinase
ATP	Adenosine Tri-Phosphate
BiFC	Bimolecular Fluorescence Complementation
CACNA1B	Calcium Channel Alpha 1B Subunit
CaM	Calmodulin
CaMKII	Calmodulin Kinase II
cAMP	Cyclic Adenine Mono-Phosphate
CNT	Concentrative Nucleoside Transporter
co-IP	co-Immunoprecipitation
C_{ub}	C-terminal half of ubiquitin
Cx43	Connexin43
Cx44	Connexin44
DAT	Dopamine Transporter
DNA	Deoxyribonucleic Acid
DnaJ	Heat shock protein 40 (Hsp40)
EGTA	Ethylene Glycol Tetraacetic Acid
ENT	Equilibrative Nucleoside Transporter
EPI	Enhanced Product-Ion scan
FAM	Fluorescein derivative
Gpbar1	G protein-coupled bile acid receptor 1
GPI	Glucose phosphate Isomerase
GSK-3	Glycogen Synthase Kinase 3
HDL	High Density Lipoproteins
HIV	Human Immunodeficiency Virus
HSQC	Heteronuclear Single Quantum Coherence
ITC	Isothermal Titration Calorimetry
LdNT2	*Leishmania donovani* Nucleoside Transporter 2
MLCK	Myosin Light Chain Kinase
MRM	Multiple Reaction Monitoring
MS	Mass Spectroscopy
MTPN	Myotrophin
MYTH	Membrane Yeast Two Hybrid
NBTI	Nitrobenzylthioinosine
NhaA	Na^+/H^+ Antiporter
NMR	Nuclear Magnetic Resonance
NOE	Nuclear Overhauser Effect
N_{ub}	N-terminal half of ubiquitin
PEG	Polyethylene glycol

PKA	Protein Kinase A
PKC	Protein Kinase C
PMAT	Plasma Membrane Monoamine Transporter
PPI	protein-protein interactions
RNA	Ribonucleic Acid
TAP	Tandem Affinity Purification
TM	Transmembrane
TROSY	Transverse Relaxation Optimized Spectroscopy
TUBB	Tubulin beta
SPR	Surface Plasmon Resonance

Chapter 1: Introduction

1.1 Importance of Nucleosides

Nucleosides are precursor molecules to nucleotides, which consist of a pentose sugar bound to one of a number of nucleobases (adenine, guanine, cytosine, uracil, and thymine) via an N-glycosidic linkage [64]. In RNA, the sugar group is a D-ribose, while in DNA, the sugar group is a 2'-deoxy-D-ribose [98]. Nucleosides are classified into two distinct categories based on the nucleobase they possess - pyrimidine or purines (Figure - 1). The pyrimidine nucleosides consist of cytidine, uridine, and thymidine [17], and the purine nucleosides are adenosine, guanosine, and inosine. The purines differ from the pyrimidines in that their pyrimidine ring is covalently bound to an imidazole ring [15]

Outside of their role in nucleic acids, the most important role of a nucleotide is demonstrated by adenosine tri-phosphate (ATP) in the cell, where it is used as an energy resource to run metabolic processes [31]. The physiological importance of nucleosides has been known for a very long time, since the late 1920's when pioneering experiments were performed to show the effects of purinergic compounds on the mammalian heart [29]. Of these purinergic compounds, adenosine seems to be in the highest abundance. Adenosine is physiologically very important in the mammalian heart and brain, especially in signalling in response to stressors such hypoxia [31, 96, 97]. The presence of nucleoside transporters in cellular membranes allows adenosine, as well as other nucleosides, to act as modulators in the cell.

Apart from being an energy store when phosphorylated, adenosine can also act as a secondary messenger when it forms a cyclic compound, 3'-5'-cyclic adenosine monophosphate, cAMP. cAMP acts as an intracellular messenger that transmits its information to a number of different proteins such as ion-gated channels. The altered cellular activity of the proteins affected by cAMP can lead to many cell functions such as calcium uptake, lipolysis, glycogenolysis, and gene expression [92].

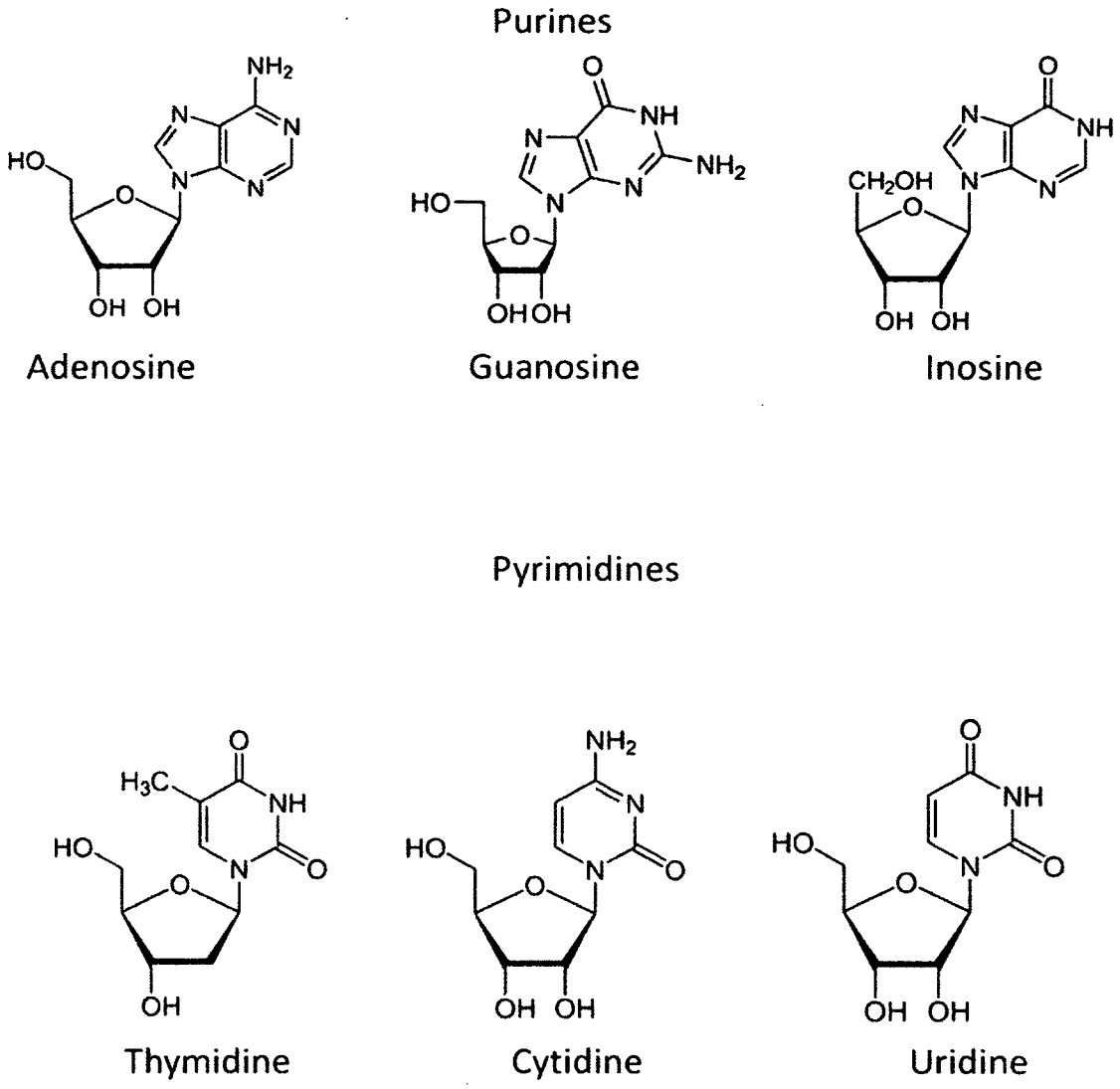

Figure - 1: Purine and Pyrimidine Nucleosides:

The more common naturally occurring purine nucleosides are adenosine, guanosine, and inosine. The pyrimidine nucleosides are thymidine, cytidine, and uridine.

1.11 Nucleoside Transporters Overview

Nucleosides, like many hydrophilic biomolecules, need to be shuttled across the plasma membrane to gain access to the interior of the cell. The concentration of both intracellular and extracellular nucleosides is determined by metabolism/catabolism as well as flux since almost all cells can synthesize nucleosides *de novo* and since there are many extracellular (membrane-bound) enzymes involved in nucleotide breakdown. The direction of uptake of adenosine by equilibrative nucleoside transporters across a cell membrane is determined by the trans-membrane concentration gradient of the nucleosides [31]. Regulation of both intracellular and extracellular concentrations of adenosine is required for homeostasis. Changes in intracellular adenosine levels can contribute to changes in cellular metabolism, such as regulation of AMP-dependent protein kinase (AMPK). When uptake of extracellular adenosine via the nucleoside transporter CNT2 is blocked by formycin B, adenosine mediated AMPK activity is hindered. This is because transport (via CNT2) and phosphorylation of adenosine is required for AMPK activity [5].

There are two families of nucleoside transporters, the integral membrane protein family of concentrative nucleoside transporters (CNTs) and equilibrative nucleoside transporters (ENTs). The CNTs comprise the SLC28 family of integral membrane proteins which are Na^+- dependent symporters [45]. The ENTs comprise the SLC29 family of integral membrane proteins which are Na^+-independent diffusion-limited transporters [7]. The predominance of these two

families of membrane proteins is, to some extent, cell specific. While the ENTs are more broadly distributed throughout many cell types, the CNTs are more cell specific, typically found in liver, intestinal and renal cells [6]. While no tertiary structures for these two families of proteins exist, their 2D topologies have been predicted (Figure - 2) [52, 95]. The development of nucleoside analogs has opened the doors to new opportunities in research to find treatments for many diseases. Nucleoside analog drugs are now routinely used for anti-cancer and anti-viral therapies and these drugs need nucleoside transporters to gain entry into the cell [77].

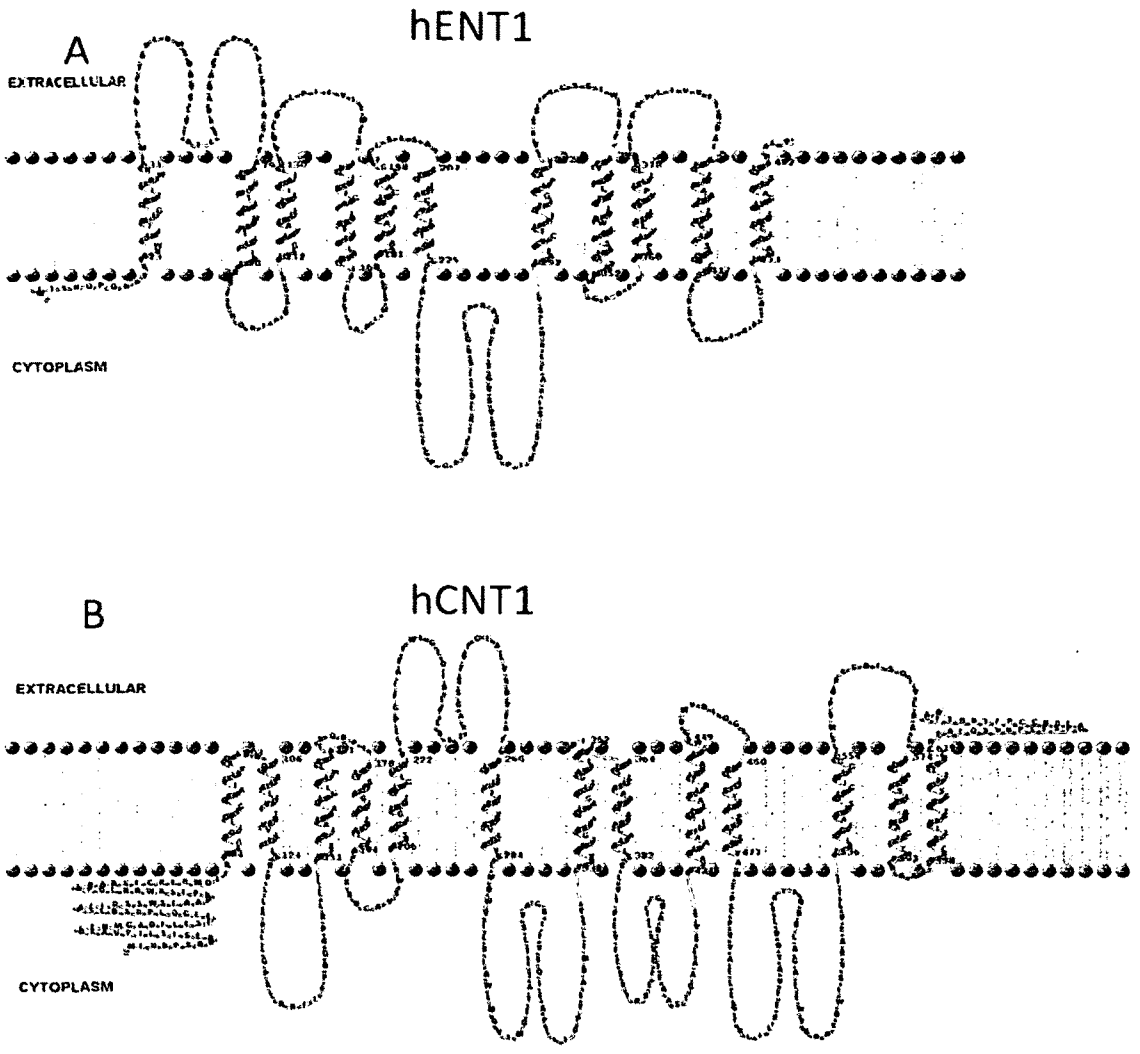

Figure - 2: Proposed 2-D topologies of hENT1 and CNT1:

A) The proposed 2-D topology of hENT1 consists of 11 transmembrane (TM) domains, with the N-terminus in the cytoplasm and the C-terminus in the extracellular space. Between TM domains 6 and 7 there is a large intracellular loop that is unstructured and free floating in the cytoplasm.
B) The proposed 2-D topology of hCNT3. CNTs are predicted to have 13 TMs, with the N-terminus in the cytoplasm and the C-terminus in the extracellular space.

1.12 Equilibrative Nucleoside Transporters (ENTs)

Four isoforms of equilibrative nucleoside transporters exist in the human SLC29 family of integral membrane proteins (hENT1 - hENT4). All four of the ENTs facilitate the transfer of nucleosides across the cell membrane by facilitative diffusion down a nucleoside concentration gradient [81]. The ENT proteins are distributed ubiquitously across mammalian cells and tissues, and, before genetic classification, they were distinguished from each other based on their sensitivity to nitrobenzylthioinosine (NBTI) [7], a high-affinity, tight-binding nucleoside analog that is not transported. In eukaryotes, mammalian ENTs are the best characterized in terms of function and structure. No homolog has been found in any prokaryote to date [52].

hENT1 (SLC29A1) is the best characterized of all the equilibrative nucleoside transporters. At 456 aa in length, it is 79% similar to its mouse homolog (460 aa), mENT1 [124]. mENT1 differs from hENT1 in that it has a splice variant lacking 6 bp, and is differentially phosphorylated. In contrast, no splice variants have been observed for hENT1 [51]. Although hENT1 is found ubiquitously in almost all cell types, it is present in greater abundance in the heart, brain, and mammary glands [48]. hENT1 transports a wide range of nucleosides down their concentration gradient, but in cardiomyocytes, it primarily transports adenosine due to its abundance. The various ENT isoforms have differential affinities for substrates and thus they will transport different

nucleosides preferentially [97]. hENT1 is primarily expressed on the plasma membrane, allowing it to transport nucleosides across the cell membrane, into the cell, from the extracellular matrix. There is evidence that hENT1 is also expressed in the endoplasmic reticulum [81] as well as being functionally expressed in the mitochondria [68], since it has a mitochondrial targeting signal [70].

hENT2 (SLC29A2) is 456 aa, has 46% similarity to hENT1 and has 79% similarity to its mouse homolog, mENT2 [25]. Unlike hENT1, hENT2 has been reported to have splice variants. One splice variant has a 40bp deletion in exon-9, which creates a premature stop codon shortening the protein to 301 aa. This truncation causes hENT2 to lose its ability to transport nucleosides [74]. hENT2 is highly expressed in skeletal muscle cells [47]. hENT2, like hENT1, transports a wide range of purine and pyrimidine nucleosides, but unlike hENT1, hENT2 can also readily transport nucleobases across the cell membrane [123]. hENT1 is highly sensitive to inhibition of uptake by NBTI (K_i = 1nM) while hENT2 is relatively insensitive to it [2].

hENT3 (SLC29A3) is 475 aa length, has 29% similarity to hENT1 and 73% similarity to its mouse homolog, mENT3 [52]. hENT3 has been shown to be predominantly localized in intracellular organelles, such as mitochondria, lysosomes and endosomes [8]. It has been suggested that the function of hENT3 in the lysosome could be to shuttle nucleosides out of the organelle following the

breakdown of RNA [8]. hENT3, unlike hENT1, but similar to hENT2, has a low sensitivity to NBTI [8]. Similar to hENT2, hENT3 transports a range of purine nucleosides, pyrimidine nucleosides, and nucleobases [8]. It has also been observed that hENT3 is functionally dependent on the pH of its environment, having an optimal pH of 5.5 [8].

hENT4 (SLC29A4) is 530 aa, and has an 86% similarity to its mouse homolog (528 residues) mENT4. Initially hENT4 was described as a low-affinity adenosine transporter [7], it was later suggested by Engel and Wang [35] that hENT4 is an organic cation transporter that does not significantly interact with nucleosides and their analogs. Subsequently, it was renamed by these investigators as plasma membrane monoamine transporter (PMAT) [35]. In 2006, Barnes *et al.* showed that hENT4/mENT4 (PMAT) could transport nucleosides at pH 5.5, unlike hENT1, which transports nucleosides at a more neutral pH of 7.4. hENT4 is ubiquitously expressed in human cells and is insensitive to NBTI [11].

The structure of hENT1 consists of 11 TM domains, with an orientation that places the N-terminal region in the cytoplasm and the C-terminal region in the extracellular space (Figure - 2) [109]. hENT1 and hENT2 are both glycosylated, on an asparagine (N) residue that occurs between TM1 and TM2. A single glycosylation occurs in hENT1 while there are two predicted sites in hENT2 [113, 116]. Functional analysis of hENT1 has been conducted by site-directed mutagenesis, where, for example, it was found that mutation of Met33 in TM1 results in a disruption of sensitivity to dipyridamole and dilazep [114]. Similarly, SenGupta et al. [102] showed that mutation of Gly179 in hENT1 to cysteine, valine or leucine, affects both transport function and sensitivity to NBTI. However, mutation of Gly179 to an alanine or a serine, hinders the ability of hENT1 to translocate to the cell membrane as well as its ability to transport nucleosides [102]. Unfortunately there is no information on the three-dimensional structure of any of the hENT/mENT proteins, although Arastu-Kapur *et al.* (2005) show a predicted tertiary structure of an equilibrative nucleoside transporter from the protozoan parasite, *Leishmania donovani*, LdNT2, that suggests that the transporter consists of a pore created by TM domains 1, 2, 4, 5, 8, 10, and 11 [4].

1.13 Concentrative Nucleoside Transporters (CNTs)

Another family of nucleoside transporters, the concentrative nucleoside transporters (CNTs), occur mainly in the liver and kidneys. The CNTs exhibit concentrative transport of nucleosides, which is Na^+-dependent and uni-directional. There are three isoforms of CNTs in the human SLC28 family of

integral membrane proteins (hCNT1-hCNT3) [45]. All of these isoforms transport nucleosides as well as nucleoside analogs; however they differ in the specificity for their substrates. CNT1 transports pyrimidine nucleosides, CNT2 transports purine nucleosides, and CNT3 transports both purines and pyrimidine nucleosides [45].

hCNT1 (SLC28A1) is primarily found in epithelia, particularly in the liver, and small intestine [68, 78]. CNT1 transports all naturally occurring pyrimidine nucleosides as well as adenosine, although transport of adenosine occurs at a much lower rate [45]. At the protein level, the human and rat homologs are 83% identical [92] and 2-dimensional topology predictions for hCNT1 show that it has 13 TM domains, unlike hENT1 which has 11 (Figure – 2) [45]. Similarly, hCNT2 (SLC28A2) and rat CNT2 are 81% identical at the protein level [86]. CNT2 in rat and humans share similar tissue distributions, such as the heart, spleen, liver and jejunum, but hCNT2 is also distributed in tissues, such as the placenta, pancreas, skeletal muscle, and colon, which is not the case for rat CNT2 [45, 86]. The most broadly selective isoform, in terms of nucleoside transport, is hCNT3 (SLC28A3), which shares 78% protein sequence to murine CNT3 [45]. CNT1 and CNT2 transport using a 1:1 ratio of Na^+ ion to nucleoside, while CNT3 uses 2:1 ratio meaning that CNT3 can transport nucleosides across the concentration gradient at a greater capacity than CNT1 and CNT2 [95].

CNTs play an important role in the homeostasis of nucleosides in the body, especially in salvage pathway of nucleosides, since transport is far more

energy efficient then *de novo* synthesis [45]. Similar to the ENTs, these transporters also play a role in the transport of nucleoside analog drugs across the cell membrane for anti-viral and anti-cancer treatment [45].

1.14 Clinical Relevance

Nucleoside transporters serve many important biological functions in the cell as discussed above, but they are also important in the treatment of many diseases. Nucleoside transporters are the route of entry of analogs of nucleosides that are used therapeutically. Nucleoside analogs have been developed as antiretroviral drugs used against diseases such as HIV and also as anticancer agents (Figure – 3) [42, 64]. Nucleoside analogs are designed to resemble their respective nucleoside, such that nucleoside transporters facilitate or enable uptake of the drug into the cell. However, once inside the cell, nucleoside analogs have a variety of effects generally aimed at promoting cell death or stopping cell profileration (Figure -4). Like many other drugs, the ability of a nucleoside analog to be effective in the cell is dependent on how much of the drug can be accumulated, which is dependent (to a considerable extent) on the presence and activity of transporter, as well as the half-life of the drug [9].

There are two main groups of nucleoside analogs; the purine-containing group (e.g. acyclovir and vidaradine) and the pyrimidine-containing group (e.g. cytarabine and fluorouracil) [22, 33, 73, 104]. Acyclovir (9- (2-hydroxyethoxymethyl) guanine, better known as ACV), is a purine nucleoside

analog that was discovered in 1977, and which was initially used as an antiherpetic agent. This approach led to a new era of treatments for diseases such as HIV. ACV became the standard for treatment of infections with the herpes virus [22]. Acyclovir is converted in a cell to acyclovir monophosphate (acyclo-GMP) via Herpes Virus-Specified Thymidine Kinase. Cellular kinases then take over metabolism of the drug and convert acyclovir monophosphate into acyclovir triphosphate. Viral polymerases then incorporate acyclo-GTP into the viral DNA, which results in chain termination of the DNA because the presence of acyclo-GTP on the DNA strand causes the polymerase to not recognize it, thereby halting the addition of further nucleotides along the chain [33]. A limitation to use of acyclovir clinically is the limited solubility of the drug in water and poor bioavailability when taken orally (10-20%), requiring a high dosage to be taken by the patient unless it is administered intravenously [22].

Another example of a purine nucleoside analog is vidarabine (1-Beta-D-arabinofuroanosyladenine, better known as ara-A), which is an analog of adenosine. Vidarabine is an anti-viral nucleoside analog prodrug that is used in the treatment of herpes viruses, rhabdo viruses, poxviruses, and RNA tumour viruses. But unlike acyclovir, it is more toxic and is unstable [104]. The mode of action of vidarabine is similar to that of acyclovir, whereby the drug inhibits the synthesis of viral DNA, especially at concentrations below those which will inhibit synthesis of cellular DNA. Unlike acyclovir, which initially uses a viral kinase in the reaction pathway that leads to phosphorylation, vidarabine uses host kinases.

This allows vidarabine to be used for mutant herpes viruses which are deficient in tyrosine kinases making them resistant to acyclovir [76].

Examples of pyrimidine nucleoside analogs include cytarabine, and fluorouracil. Cytarabine (arabinofuranosyl cytidine, better known as Ara-C) is an analog of cytidine [83] and is mainly used in the treatment of cancers such as acute myeloid leukemia (AML) and non-Hodgkin lymphoma [115]. Like other nucleoside analog drugs, cytarabine interferes with DNA synthesis [12, 85] and like many other nucleoside analog drugs, high doses or frequent administration of cytarabine can lead to spinal cord toxicity [117]. Fluorouracil (fluoropyrimidine 5-fluorouracil, better known as 5-FU) is a nucleobase that inhibits both DNA and RNA synthesis. 5-FU is an analog of uracil that has a fluorine atom at the C-5 position and like the nucleoside analog drugs; it goes through a series of modification steps until it has a triphosphate group, which allows incorporation into RNA [73].

Finally, parasitic organisms such as those in the genus *Plasmodium* cause a disease known as malaria. Deletion of *LdNT1*, the nucleoside transporter 1 gene, is a novel method for vaccine creation [1]. Unlike their hosts, malaria parasites do not have the biochemical machinery to synthesize their own nucleosides and require uptake of nucleosides via their NTs. Therefore, deletion of parasitic NT1 does not allow for the organism to duplicate its genome for replication. By doing so it becomes attenuated and cannot multiply to high

enough numbers to cause malaria and can be cleared by the hosts immune system. Since its ability to replicate and therefore its ability to cause disease has been halted, *Plasmodium* can therefore can be used for vaccine creation [1].

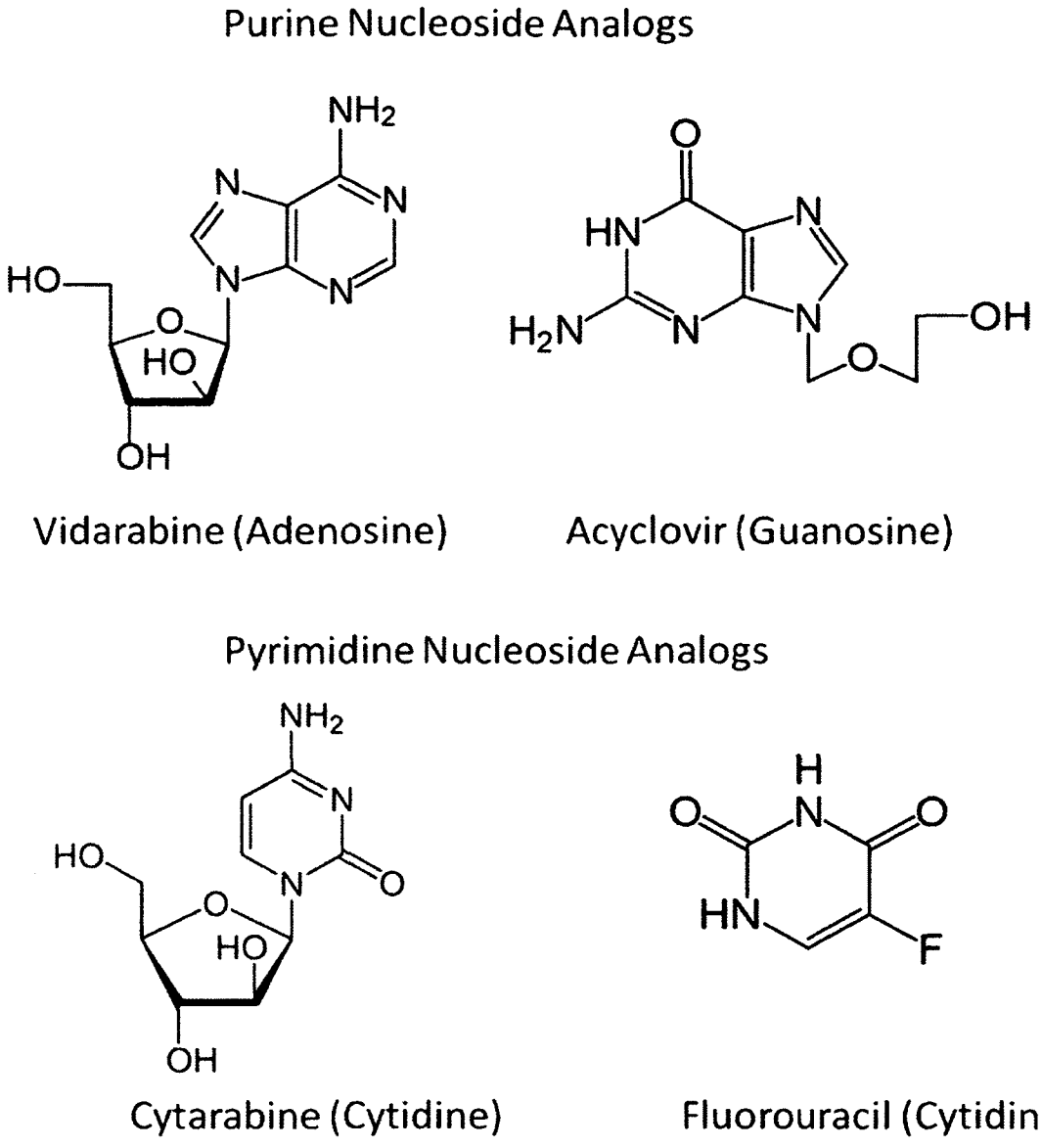

Figure - 3: Structures of Clinically Important Nucleoside Analogs:

Nucleoside analogs are designed to resemble their respective nucleoside so that nucleoside transporters will transport them into the cell while modification of the structure results in a significant intracellular event such as chain termination. Examples of purine nucleoside analogs include vidarabine and cytarabine while nucleobase analogs included acyclovir and fluorouracil.

1.15 Phosphorylation and Regulation

Protein phosphorylation is an essential posttranslational modification for many proteins. Phosphorylation can dictate the role a protein may have in a multitude of different cellular processes. The addition of a phosphate group occurs most prevalently on serines, threonines, and tyrosines in eukaryotes and on arginine, histidine and lysine in prokaryotes [10, 24]. Phosphorylation of proteins is reversible in both eukaryotes and prokaryotes and is an important regulatory mechanism [18, 108].

Approximately 2% of the human genome encodes protein kinases. Two examples of kinases are protein kinase A (PKA) and AKT [41, 110]. PKA is one of the best described kinases and its activity is dependent on the levels of cAMP within the cell [110]. AKT is a serine/threonine kinase that has a key role in the cell cycle and apoptosis. Three members of AKT kinases (akt1-3) exist, each having an expression pattern that is tissue specific. Since an important role of AKT kinase in healthy cells is the regulation of apoptosis and cell proliferation, cells which are defective or deficient in AKT kinase have a higher probability of becoming malignant than normal cells [41].

Kinases all share a conserved structurally similar kinase domain [101]. Phosphorylation can lead to regulation of kinases. For example, phosphorylation of Ser9 of glycogen synthase kinase 3 (GSK-3) by ATK causes it to become inactive; GSK-3 has an important role in cellular metabolism and the insulin pathway [118]. The proto-oncogene tyrosine-protein kinase Src plays an important role in cancer biology. The activity of Src can be affected by

phosphorylation when a protein kinase, Csk, phosphorylates Src causing a conformational change in the structure of Src, thereby inactivating it [23]. Phosphorylation of p53 tumour suppressor also plays an important role in cell cycle, proliferation and apoptosis. More than 18 sites exist on p53 along the C and N – termini which can be phosphorylated, allowing for regulation of this protein. Interaction between proteins, based on how stringently they bind to each other, is also affected by phosphorylation. One example is a member of splicing factors in the SR protein family, ASF/SF2, which, when phosphorylated, significantly increase their binding affinity to their protein partners [122]. Lastly, protein degradation via ubiquitin has also been implicated as being regulated by phosphorylation. For example, when c-Myc, a protein involved in cell growth and division, is phosphorylated on threonine-58, it allows Fbw7 to bind to it, which, in turn, mediates protein degradation [120].

There is also evidence for regulation of transporters by phosphorylation. For instance, the glutamate transporter, GLT1, is phosphorylated on serine-133 as well as being glycosylated. When astrocytes or C6 astrocytoma cells are exposed to activators of PKC, the transporter is phosphorylated resulting in an increased uptake of glutamate [43]. The dopamine transporters (DATs) are a family of neurotransmitter transporters found at synaptic clefts and responsible for the rapid transport of dopamine. Vaughan *et al.* (1997) showed that DATs are readily phosphorylated following activation of PKC and that dopamine transport in synaptosomes was diminished after DAT phosphorylation [119].

It has already been established that hENT1 is phosphorylated [90]. The next challenge is to identify the kinase(s) that participate and to determine the identity of the phosphorylation sites. Recent data from the Coe lab has identified Ser88 as the predominant phospoacceptor [90].

It is worth noting that as more phosphoacceptor sites are identified in hENT1, the diversity in its regulation substantially increases. Since a phosphorylation site can either be "on" (with a phosphate group) or "off" (dephosphorylated) the system becomes 2^N combinations, where N is the number of sites that can be phosphorylated [99]. For example, if a given protein has 8 phosphorylation sites, there are a total of 256 possible phosphorylation states. Multisite phosphorylation can occur in 4 categories; either randomly, sequentially - where phosphates are added in the order they appear on the protein sequence, cyclically - whereby the last amino acid to gain a phosphate group is also the first to lose it, and lastly, in a hierarchical manner, where the next amino acid cannot be phosphorylated until the preceding one has first been phosphorylated [99].

1.2 Protein-Protein Interactions

Protein-protein interactions (PPIs) are not only functional in their nature, but also present a direct means of communicating a signal in a cell. Much of systems biology is devoted to identifying and connecting PPIs in new pathways to understand cellular function at a global level.

One method that is considered one of the gold standards for detecting novel protein-protein interactions is co-immunoprecipitation (co-IP). This process involves precipitating bound proteins, usually from a cell lysate [13]. An antibody bound to gel beads is typically used to bind to the protein of interest and any resulting interaction is also "pulled down" such that the resulting interaction can then be identified by western blot. If an antibody against the binding partner is used for immunoblotting and generates a signal on a western blot, this suggests an interaction is present. While being a widely used method for PPI detection, co-IPs do have some drawbacks. Any bands that are identified on a blot may suggest an interaction, but may also be due to aggregation or non-specific interaction of much larger complexes. Co-IP is also not a quantitative methodology and is not as sensitive as some other detection methods [80].

Another method which is can be used to validate PPIs is biomolecular fluorescence complementation (BiFC). This method allows for the detection of protein-protein interactions via fluorescence in living cells. The system works by taking a fluorescent protein, and in essence, splitting it into two forms which no longer fluoresce. The non-covalent interaction of the two halves will allow the fluorophore to fluoresce, which denotes an interaction has taken place [63]. One advantage this technique relative to other detection platforms is its sensitivity and its ability to detect weak interactors, as well as proteins that are expressed at low levels [36]. Limitations for BiFC include the requirement of use of fusion proteins,

which may hinder the true function of the proteins, and affect the localization of the protein within the cell, and the interaction with endogenous partners [63].

Tandem affinity purification (TAP) is another method which is used to identify protein-protein interactions. The TAP tag, which encodes a calmodulin binding site, two IgG binding domains, and a TEV cleavage site, is fused to the cDNA of the protein of interest. This fusion protein is expressed in the cell at close to its natural levels. The cells are then lysed and the lysate is passed over an IgG column. The bound fusion proteins are released from the column by cleavage via a TEV protease. The eluent is run through calmodulin affinity beads and the resulting bound fusion proteins are eluted with EGTA. The resulting fusion proteins can now be examined for binding partners [93]. The main advantage to TAP is that no prior knowledge of the protein complexes is needed to identify protein interactions *in vivo* [87].

1.2.1 Membrane Yeast Two Hybrid

The previously described methods are excellent for identifying protein-protein interactions that are mainly cytosolic. Detection of PPIs of membrane proteins requires another approach, which takes into account their inherent hydrophobicity [107]. Membrane proteins make up approximately one-third of all proteins in a cell, having important functions in signalling, cell structure, and, as discussed above – transport. Membrane proteins are distributed ubiquitously and understanding their PPIs has important implications in medicine since many membrane proteins are drug targets [34].

In 1994 a split-ubiquitin based method was established by Johnsson and Varshavsky [60], when they discovered that ubiquitin, split into two moieties, can reassociate due of the high affinity of the moieties for each other. These two halves were named Nub for N-terminal half of ubiquitin, and Cub for C-terminal half of ubiquitin [60]. These researchers fused cDNAs encoding a library of proteins to the N-terminal moiety called Nub. Two variants of Nub are used. NubI refers to the wild type form bearing Ile13. The NubG form bears an Ile13 Gly substitution. This substitution ensures that the affinity between Cub and Nub is decreased such that if the bait and prey interact, Cub and NubG will be forced together and ubiquitin-specific proteases will recognize the complete ubiquitin molecule and cleave off the reporter protein from Cub, which can be detected through selective screening [60].

This simple, but elegant method for the detection of protein-protein interactions for integral membrane proteins was later adapted for high-throughput screens and this system came to be known as Membrane Yeast-Two Hybrid, MYTH (Figure – 4). The membrane protein of interest is bound to the C or N-terminal moiety of Cub. Cub is fused to transcription factors, which consist of DNA-binding domain LexA from *Escherichia coli* and VP16 from the herpes simplex virus. This Cub fusion protein is known as the bait. The prey is a NubG-fused cDNA library. Both the NubG and Cub fusion proteins are co-expressed in yeast. If an interaction takes place with the bait and the prey, ubiquitin-specific proteases will recognize the complete ubiquitin molecule and cleave off the

transcription factors from Cub. The transcription factors then translocate to the nucleus and activate the reporter genes: LacZ, His3, Ade2 [105]. While MYTH is, by far, the best tool available for examining PPIs of membrane proteins, it does have disadvantages: A high number of false positives can arise during screening, although this can be somewhat alleviated by making more stringent growing conditions for the yeast, as well as performing subsequent bait dependency tests to confirm the validity of the interaction. The putative interacting preys are re-screened against the bait as well as non-interacting artificial bait and if an interaction occurs with the artificial bait, it is said to be a false positive and the putative prey protein is discarded [57].

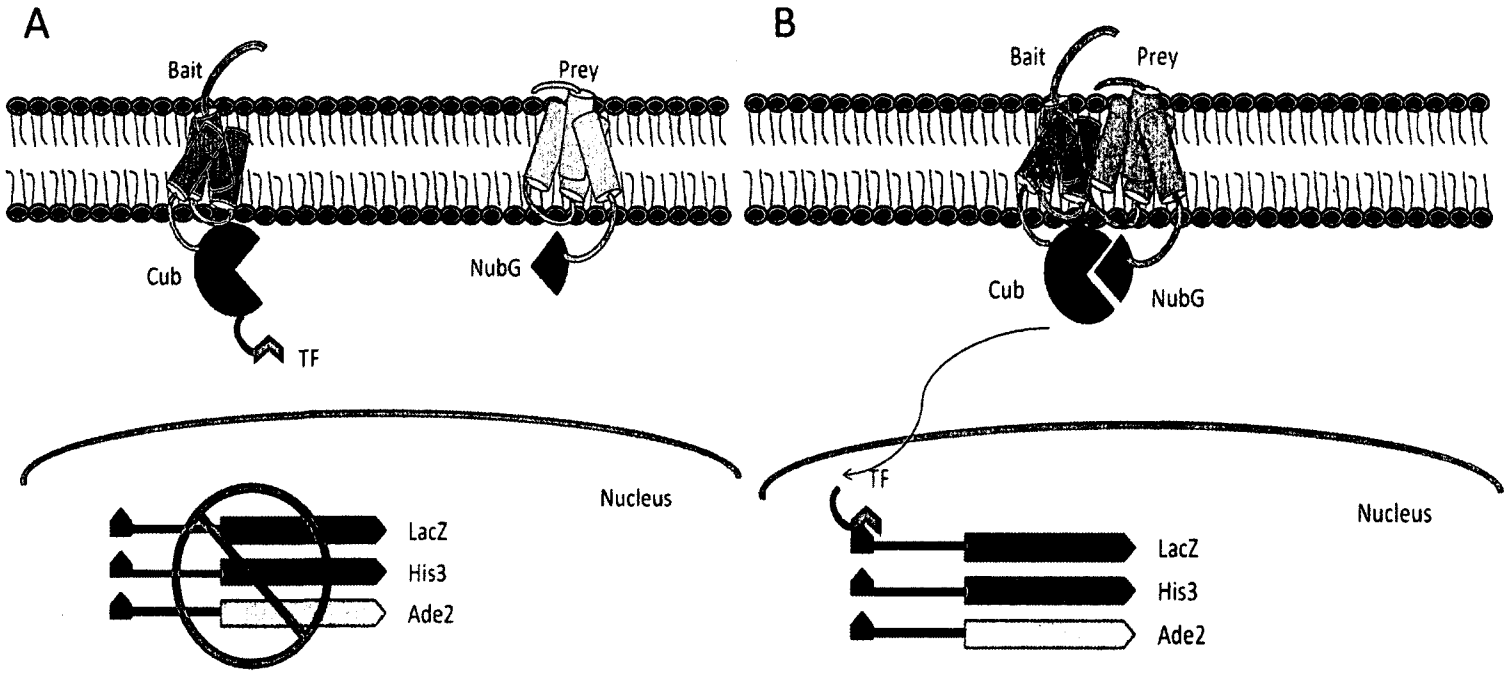

Figure - 4: MYTH:

Split-Ubiquitin Based Membrane Yeast Two-Hybrid (MYTH). The protein of interest (Bait) is fused to the C-terminal half of ubiquitin (Cub), while the Prey protein is one of a number of different proteins from a cDNA library, which is subsequently attached to the N-terminal half of ubiquitin (NubG). A) If no interaction between the bait and the prey takes place, then the reporter system will not be turned on. B) Only when an interaction takes place are the two halves of ubiquitin forced together resulting in ubiquitin specific proteases cleaving off the transcription factor attached to Cub and turning on the reporter system.

1.2.2 Nuclear Magnetic Resonance

Nuclear magnetic resonance (NMR) spectroscopy is tool used by chemists and biologists to conduct structural analyses of molecules, including proteins [59]. In the presence of an external magnetic field, nuclei with a spin quantum number of 1/2 will align with or against the field. The energy difference between the two states is proportional to the strength of the magnetic field and follows a Boltzmann distribution [59]. Even in a strong magnetic field of 19 T, the energy difference dictates that only a few thousand of a percent of the nuclei will populate the lower state in excess. Thus NMR is relatively insensitive form of spectroscopy. To improve the signal to noise of spectra, protein samples are typically in the range of 1 mM, or 10 mg/mL for a 10 kDa molecule. The common spin 1/2 isotopes in biomolecules are ^{1}H, ^{13}C and ^{15}N [53]. Since the natural abundance of ^{13}C and ^{15}N is very low, bacteria are fed a medium consisting of these nonradioactive nuclei as their sole sources of carbon and nitrogen.

A folded protein is an amalgamation which provides a rich electronic environment, which is consequently manifested as a rich magnetic environment. Hydrogen bonds and proximity to aromatic rings are two examples that contribute to this environment [121]. As a result, not every ^{1}H, ^{15}N and ^{13}C in the protein experiences the same magnetic field and a spectrum results. Protein binding and conformational changes affect the magnetic/electronic environment of the protein, which, in turn, can be read out in spectral changes [121, 59]. A protein structure is determined by identifying peaks in spectra that arise from a property

called the Nuclear Overhauser Effect, or NOE. A NOE occurs when two ^{1}H are within 5 Å of each other and exchange energy. But identifying and measuring the intensity of thousands of NOEs acting like tiny molecular rulers, a protein structure can be calculated [121].

In this thesis, I have monitored chemical shift changes in ^{1}H and ^{15}N that directly read out structural changes in calmodulin as it interacts with ENT1 peptides.

1.2.3 Binding Parameters

Understanding the interactions that take place within a cell, either ligand-protein, protein-protein etc, requires detailed knowledge of the thermodynamic properties of the interactions, such as the dissociation constant (K_d), which is important for understanding binding affinity [75]. The dissociation constant is primarily used to describe the non-covalent binding affinity of a protein and a ligand, such as hydrogen bonding, Van der Waals forces, and electrostatic interactions. The dissociation constant is represented by the following equation [21]:

Kd = [L]*[P]/ [LP}

[L] = the concentration of the ligand

[P] = the concentration of the protein

[PL] = the concentration of the protein-ligand complex

Binding affinity can vary greatly depending on the two substances that are interacting. For example, the binding of morphine and μ-opiate receptor (1.5×10^{-9} M) is in the nM range, while weaker interactions occur between enzymes and their substrates, in the μM range [30].

1.2.4 Binding Parameter Detection Platforms

Determining the dissociation constant for protein-protein interactions can be done by a number of different methods. One method is Isothermal titration calorimetry (ITC). ITC is a very robust method for determining thermodynamic properties of molecular interactions, as well as reaction stoichiometry [100]. ITC works by measuring the heat either given off (exothermic) or absorbed (endothermic) during binding between two molecules. Measurements are made with an isothermal titration calorimeter, which is composed of two cells, sample and reference, surrounded by an adiabatic shield. Either the ligand or the protein is placed in the sample cell and the other is placed in the injection syringe. The syringe injects into the sample cell a controlled volume at a designated time interval. The syringe also aids in the mixing of the sample cell. The temperature is constantly measured after every injection and compared to that of the reference cell. Data are presented in the form of plot and an appropriate model is derived to obtain the thermodynamic properties of the interaction [111]. ITC has gained a lot of popularity over the years due to its ease of use and its ability to obtain thermodynamic properties of protein-protein, DNA-protein and RNA-

protein interactions [71]. One limitation of ITC is that it requires the use of potentially milligram amounts of each component, depending on calorimeter being used.

Another method for determining binding constants is Surface Plasmon Resonance (SPR). SPR works by immobilizing the protein of interest on a dextran matrix which, in turn, rests on a gold film. The analyte is allowed to flow over the dextran surface in a controlled manner [14]. When the gold particles under the dextran matrix are irradiated with lasers of a specific wavelength, the gold begins to oscillate creating surface plasmons. When an incident light wave matches the wavelength of the surface plasmons they resonate, decreasing the amount of light reflected off the surface. The angle at which this occurs is known as the surface plasmon resonance angle. A detector measures the decrease in the angle of reflected light and any changes that may occur in real time if an interaction occurs on the dextran surface between a ligand and protein, which would cause a change in the SPR angle [84]. The intensity of this reflected light is measured and analysis of the molecular interactions can be made. One advantage SPR has is that it uses a minimal amount of material to obtain a dissociation constant relative to that of ITC.

Lastly, fluorescence anisotropy is another method for measuring biomolecular interactions. Fluorescence anisotropy, unlike ITC and SPR, requires a fluorescent moiety such as fluorescein bound to one of the ligands, typically the smallest one (a peptide in the case of this thesis) [16]. The assay

measures anisotropy which is the ratio of polarized light emitted from the fluorophore relative to the total light. When the oligonucleotide is bound to the protein of interest, the rotational correlation time (the time it takes the protein to rotate one radian) increases because of the resulting size change of the complex, this increase in size results in a change of emitted light from the fluorophore [69].

1.3 Thesis Rationale

The main objective of my thesis was to identify interacting partners of hENT1. Therefore, I propose to use MYTH to identify novel interacting putative partners. Interactions of interest can be confirmed via biochemical assays such as bait-dependency screens and specific interactions can be further investigated using innovative biochemical approaches such as NMR and fluorescence anistropy. These approaches have never been used before, to our knowledge, in the investigation of hENT1 structure and function and results from these studies will give insight into the fundamental biology of hENT1. Moreover, our lab has recently discovered that the serines in the large intracellular loop in both hENT1 and mENT1 have the potential to be phosphorylated. Investigation of these phosphorylation sites with new mass spectrometry techniques, such as multiple reaction monitoring assays, can give new insight into the cellular regulation of these clinically important proteins.

Chapter 2: Methods and Materials

2.1 Membrane Yeast Two Hybrid (MYTH)

2.1.2 Bait Construction and Expression

Cloning of mENT1 into a MYTH vector, pTLB-1 (Dualsystems Biotech AG, Schlieren, Switzerland) allows for the bait protein to be fused to the N-terminal region of the Cub transcription factors. To achieve this, mENT1 cDNA was amplified from its host plasmid by standard PCR using Phusion® High-Fidelity DNA Polymerase (New England Biolabs, Ipswich, MA). The hENT1 cDNA was then ligated into both MYTH vectors via homologous recombination via a standard yeast transformation [39]. Two yeast strains were used, L40 (MATa his3-200 trp-901, leu2-3 112 ade2, LYS2::(4xlexAop)-HIS3, URA3::(8xlexAop)-lacZ GAL4) [39] and THY.AP4 (MATa leu2, ura3, trp1 :: (lexAop- lacZ) (lexAop)-*HIS3* (lexAop)- ADE2) [65]. The strain THY.AP4 is used for homologous recombination since it grows faster and stays alive longer at 30 °C. Greater quantities of MYTH plasmids were obtained by transformation of the plasmid into *E. coli* using a transformation kit with NovaBlue competent cells (EMD Chemicals Darmstadt, Germany). To check for self activation of the MYTH vectors with mENT1 cDNA, NubG/NubI tests were performed whereby yeast carrying the hENT1 MYTH vector was transformed with control plasmids (Fur4 NubI and Ost1 NubI [Positive control], Ost1 NubG and Fur4 NubG [Negative control]) by standard yeast transformation. Following growth on SD-WL plates, a range of serial dilutions from 1:100 - 1:10000 was performed and samples spotted onto

SD-WLAH plates with varying amounts of 3-amino-1,2,4triazole (3-AT), up to 100mM and allowed to incubate at 30 °C for 2-5 days.

2.1.3 Prey Construction and Expression

All mENT1 clones were obtained from a size-selected yeast cDNA library containing 1.5 x 10^6 independent clones in the vector pPR3-N with an insert size of 0.6 – 10kb and an average insert size 1.1kb. The NubG-X library was derived from 11 day whole mouse embryo NubG-X and obtained from Dualsystems Biotech AG, Schlieren, Switzerland). The NubG-X library was diluted to 60 ng/µl and transformed into DH5α library-competent cells (using 8 duplicate aliquots of 100µl of cells in15 mL of LB transformations) and plated onto 15 cm LB-Amp plates. After 24 hours of growth, plates were scraped and standard "maxi" preps were performed (PureLinkT HiPure Plasmid Filter Maxiprep Kit) to obtain plasmid at concentrations exceeding 1 µg/µL for further analysis. Standard Yeast transformations were performed to assess library quality and efficiency.

2.1.4 MYTH Assay

Myth assays were performed as previously described [106]. In brief, the yeast strain THY.AP4 (MATa leu2, ura3, trp1 :: (lexAop- lacZ) (lexAop)- HIS3 (lexAop)- ADE2) was transformed with the mENT1 pTLB-1 bait plasmid and the 11 day whole mouse embryo NubG-X prey plasmid using the lithium acetate method [44], and plated on SD-WL plates. Colonies were selected based on size

and shape, diluted in 100 µL of ddH_2O and spotted onto SD-WL and SD-WLAH +/- 3-AT X-Gal plates. Any colonies that grew and exhibited β-galactosidase activity was scored as an interaction between the bait and prey.

2.1.5 MYTH Assay DTT Method

Myth assays were also performed using a modified version of the DTT yeast transformation method – original method described by Chen *et al.* in 1992 [19]. Yeast strain THY.AP4 (MATa leu2, ura3, trp1 :: (lexAop- lacZ) (lexAop)- HIS3 (lexAop)- ADE2*)* was grown overnight until stationary phase. Cells (25ml) were spun down and mixed with buffer [lithium acetate, 50 mM; PEG 3350, 40%; dithiothreitol (DTT), 100 mM; single stranded carrier DNA, 2 mg; 10-15 µg of NubG-X prey plasmid library] for a total volume of 12 mL. After creating the mixture, the culture was divided up into 3-4 mL in 15 ml Falcon tubes and heat shocked in a 45 °C water bath for 30 min. The cell mixtures were pooled and spun down at 700g for 5 min. The pellet was resuspended in 2 x YPAD (12 mL) and allowed to recover for 1hr at 30 °C. The cell mixtures were spun down at 700 *g* for 5 min, diluted into 0.9% (w/v) NaCl and plated onto SD-WLAH plates with 120mM of 3-amino-1,2,4triazole (3-AT), as well as 3 serially diluted plates from 1:100 - 1:10000 to check for transformation efficiency. These plates were allowed to incubate at 30 °C for 2-5 days.

2.1.6 Prey Validation

Positive prey plasmids that were selected from the positive colonies obtained from the MYTH screens were retransformed into THY.AP4 yeast with mENT1 pTLB-1 bait plasmid, as well as control bait plasmid that consisted of an artificial bait protein which will not interact with any protein. The transformants are plated serially in triplicates on SD-WL and SD-WLAH X-GAL plates with 100 mM 3-AT. Colonies that showed β-galactosidase activity in both the mENT1 and artificial bait transformants were determined to be self activating and discarded. Those that did not show self-activation were selected for further screening using functional assays.

2.1.7 Bioinformatic Prey Analysis

Calmodulin was identified as one protein partner of hENT1. The hENT1 sequence (GI:1845344) was analyzed and compared to known calmodulin interactors in the Calmodulin Target Database [125, http://calcium.uhnres.utoronto.ca/ctdb/ctdb/sequence.html]. The mENT1 sequence (AF131212) was also analyzed.

2.1 NMR Analysis

2.2.1 Protein Expression

A chimeric gene encoding the large intracullular loop of hENT1, residues 228-290, in tandem with a 6xHis-ubiquitin tag, and an intervening thrombin site, was designed and commercially synthesized in a the expression vector ,

pJexpress 401 (DNA2.0 / Menlo Park, CA). A human calmodulin (CaM) clone was provided by Dr. Mitsu Ikura (University of Toronto, Toronto, ON) and consisted of the CaM cloned into a pET15b with 6xHis tagged and an interpolated thrombin site at the N-terminal.

CaM fusion peptides were expressed in a conventional M9 minimal media (in 1L batches) with ^{15}N-ammonium chloride as the only source of nitrogen while the 6xHis-ubiquitin-hENT1 loop proteins were expressed in LB-Kan in a culture of *E. coli* BL21:DE3 cells. The cells were grown to an OD_{600} of 0.8 and then induced with IPTG for 3 hours. Cells were then centrifuged (10000 x g for 10min) and lysed with a French press. The fusion peptides were purified from the cell lysate by a combination of standard nickel affinity and gel filtration chromatography.

2.2.2 NMR Measurements

Uniformly ^{15}N-labeled CaM at 0.12mM in PBS, supplemented with 10% D_20 and 3μM of $CaCl_2$ was titrated with 6xHis-ubiquitin-hENT1 at a 1:2 ratio in a ^{15}N-edited HSQC spectra (768x80 pts) were acquired on a 600 MHz Varian NMR spectrometer

2.3 Anisotropy

Fluorescence anisotropy measurements were made with a Cary Eclipse Fluorescence Spectrophotometer. Measurements were performed at room

temperature. The titrations were carried out with 1x PBS stock (NaCl, 137 mM; KCl, 2.7 mM; $Na_2HPO_4 \cdot 2\ H_2O$, 10 mM; KH_2PO_4. 1.76 mM; pH ~7.4) and 3μM of $CaCl_2$ and the large intracellular loop of hENT1 at 0, 2, 4, 8, 16, 32, 64, 75, 95 mM aliquots. Analysis was done using a fluorescently tagged peptide consisting of the putative CaM binding site in the large intracellular loop of hENT1 (residues 224 – 245) plus 3 C-terminal lysines added to enhance solubility as well as a PEG spacer, and a fluorescein derivative (FAM) tag (CanPeptide Inc, Pointe-Claire, Québec).

5-FAM-PEG-LGLPRLEFYRYYQQLKLEGPGKKK

The peptide was kept at a constant 2μM during the titrations. Fluorescence anisotropy was measured at an excitation wavelength of 494.0 nm and an emission wavelength of 523.0 nm.

Anisotropy, R, is measured using the equation below, whereby I_{vv} is with both polarizer's in the vertical position, and I_{vh} is with the perpendicular polarizer in the horizontal position, and G is the G-factor.

$$R = (I_{vv} - G * I_{vh})/(I_{vv} + 2 * G * I_{vh})$$

A total of three runs were performed and an average of the relative anisotropy was fit to the following the two-component binding function:

```
y := 0.5*a[3]*((x+a[1]+a[2]) - Sqrt( ((x+a[1]+a[2])*(x+a[1]+a[2])) - (4*x*a[1]) ) )

  a[1] := protein concentration
  a[2] := Kd
```

a[3] := 1, constant to simulate all available binding sites

2.4 Phosphorylation assay

Phosphorylation assays were performed on over-expressed purified large intracellular loop of hENT1 and mENT1-loop; the same construct used for NMR analysis. Peptide (10µg) in 1x buffer stock ($MgCl_2$, 10 mM; $CaCl_2$, 100 µM; Tris-HCL, 25 mM; pH ~7.0) was mixed with PKA (catalytic subunit from mouse; 5000 units) and non-radiolabeled 100µM ATP. Samples were incubated at 30 °C for 2-5 hrs and then separated by SDS-PAGE (150V, 2hrs).

Samples were either extracted from the SDS-PAGE gel slice or the incubated samples that were not run on the SDS-PAGE underwent an in solution trypsin digest, and were then analyzed using MRM-triggered EPI scan.

Chapter 3: Results

3.1 mENT1 MYTH Results

Murine ENT1 was the first nucleoside transporter to be tested in the split ubiquitin membrane yeast two-hybrid screen. To generate the mENT1 bait, the full length murine ENT1 protein was fused C-terminally to the Cub reporter cassette which contains LexA-VP16-Cub generating mENT1-LexA-VP16-Cub (Figure – 5a). I then examined whether the mENT1 bait was self-activating by transforming with the yeast protein Fur4 [105] fused to either NubI or NubG. Growth observed with co-expression of Fur4-NubI but not Fur4-NubG would indicate that the bait is not self-activating (Figure – 5b).

To identify novel interactions with the mENT1 bait, MYTH screens were performed on the NubG-X 11 day whole mouse embryo library. The majority of the clones generated through the MYTH screens were false positives. False positives arise because the system uses fusion proteins (bait protein Cub cassette and the cDNA library NubG cassette), which are overexpressed outside of its host organism [103]; these false positives have also been observed in standard yeast two-hybrid systems [105]. The clones underwent bait validation with bait dependency, whereby the putative prey proteins were re-transformed with the mENT1 bait as well as an artificial bait plasmid (Figure - 6). Six preys that interacted with the mENT1 bait from the bait dependency screen were identified as CALM1, GPI, TUBB, DnaJ, MTPN and Gpbar1 (Table - 1).

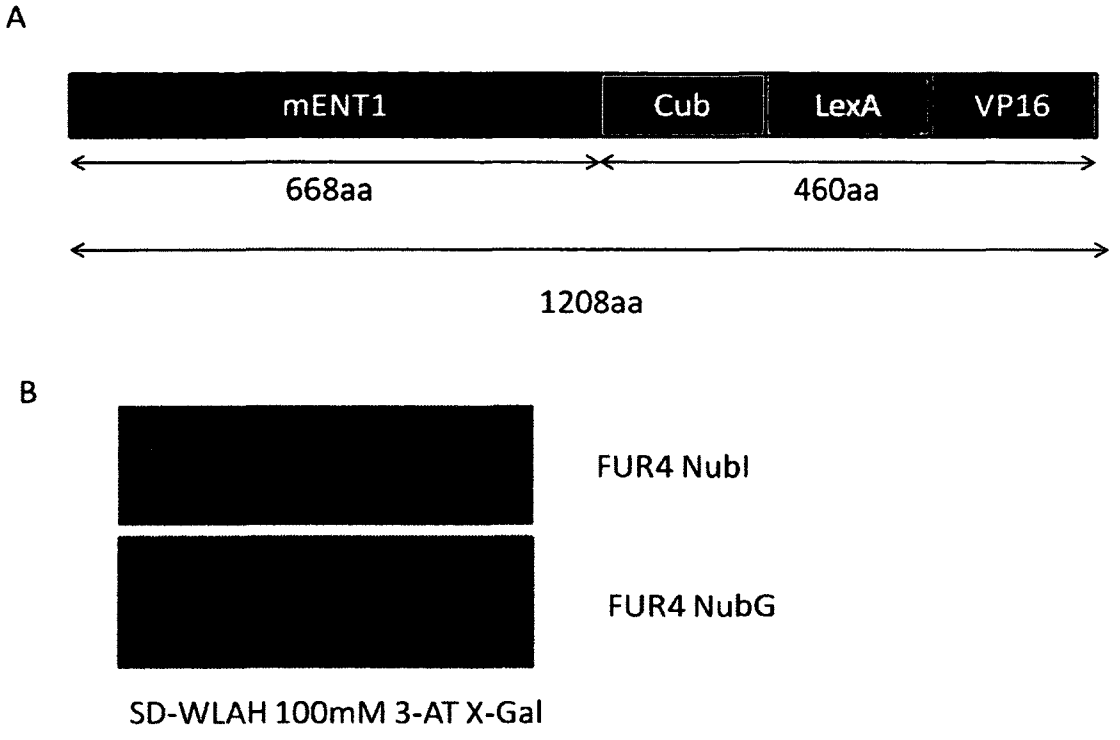

Figure - 5: mENT1 bait:

A) The structure of the mENT1 pBT3-N bait protein. mENT1 is a type II transmembrane protein, whereby the C-terminal region is outside of the cell (type I transmembrane proteins in which the C-terminal region is in the cytosol).The mENT1 protein is fused to the N-Terminal end of Cub which is fused to the transcription factors LexA and VP16. The number of amino acids of the complex is indicated. B) THY.AP4 yeast cells were grown expressing the mENT1 bait plasmid on SD-WLAH X-Gal plates with 100mM of 3-aminotriazole (3-AT), co-expressing FUR4 NubG/I. Growth and β-galactosidase activity for FUR4 NubI but not FUR4 NubG indicates that the bait is not self-activating.

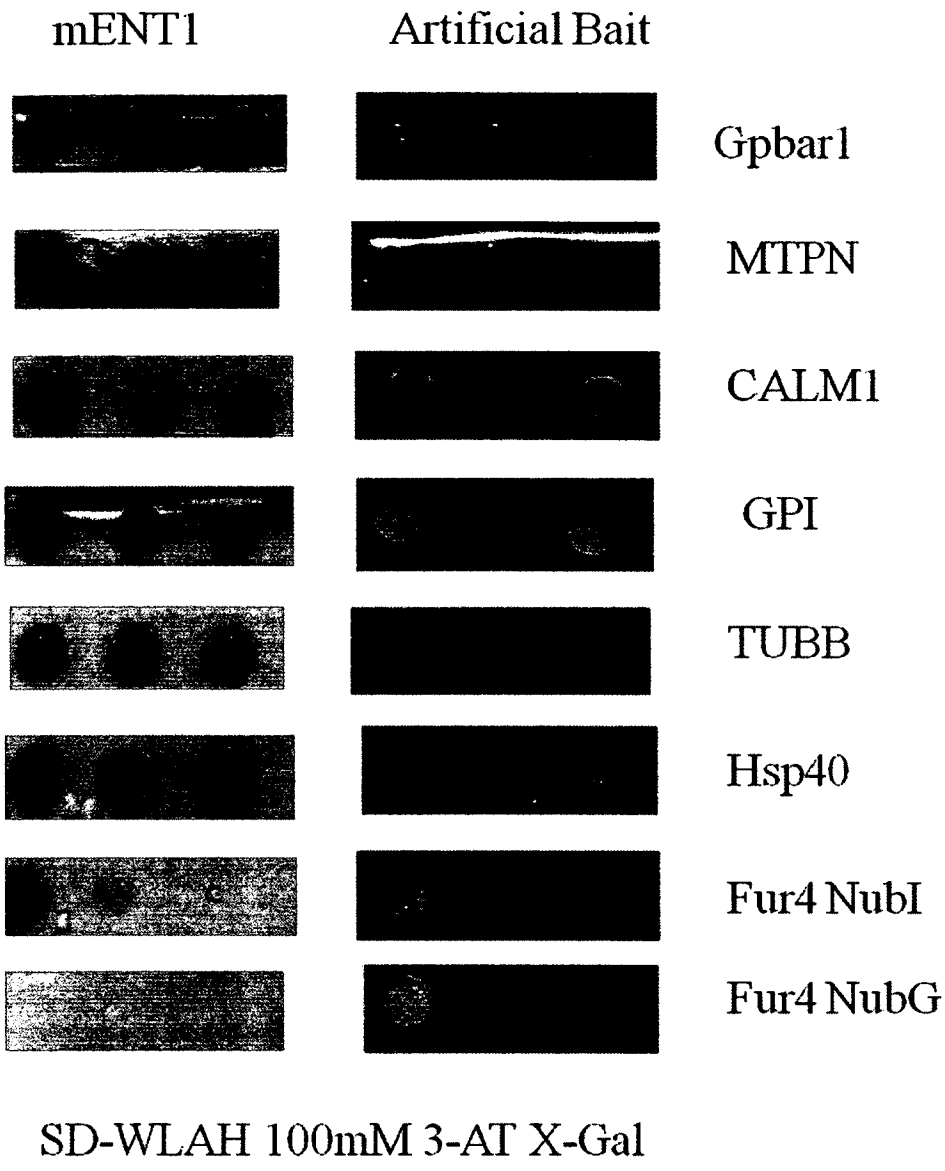

Figure - 6: Bait dependency screen of mENT1 interacting partners:

Novel split ubiquitin membrane yeast two hybrid interactions. Positive prey are retransformed into THY.AP4 yeast cells with the mENT1 bait plasmid as well as an artificial bait. Growth and β-galactosidase activity on the mENT1 bait but not on the artificial bait show novel interactions through MYTH. Fur4 NubI/G are used as controls to show that the bait plasmids are not self activating.

Table-1: Novel putative mENT1 interacting partners identified by MYTH

Interacting Partner Gene Name	Accession Number	Cell Location	References
G protein-coupled bile acid receptor 1 (Gpbar1)	NM_174985.1	Cell Membrane	[39]
Myotrophin (MTPN)	NM_145808.3	Cytoplasm, Nucleus	[69]
calmodulin 1 (phosphorylase kinase, delta) (CALM1)	NM_006888.3	Cytoplasm	[54]
glucose phosphate isomerase (GPI)	NM_000175.2	Cytoplasm	[46]
tubulin, beta (TUBB)	NM_178014.2	Cytoskeleton	[50]
DnaJ (Hsp40)	NM_001539.2	Cytoplasm	[88]

3.2 Bioinformatic Prey Analysis

3.2.1 hENT1 Binding Residues

The potential for hENT1 to bind to calmodulin was investigated using the Calmodulin Target Database [125]. A putative binding site was found between residues 224 -244. This region of the hENT1 protein is within the long unstructured loop situated in the cytoplasm between transmembrane domains 6 and 7 [89]. CaM binding sites are based on potential binding to bulky hydrophobic residues such as Phe, Val, Ile, Leu, or Trp, in a number of different motifs [91]. We found that putative binding of CaM to hENT1 most closely corresponds to a 1-5-10 consensus motif defined as xxx(FILVW)xxxx(FAILVW)xxxx(FILVW). Computational analyses of hENT1 and mENT1 sequences and comparison to other known CaM binding partners support a 1-5-10 motif (Figure – 7a). Although none of the binding sites show perfect homology to each other, they all share a similar consensus motif, demonstrating that CaM has the ability to bind to a multitude of different proteins.

To determine whether CaM can also putatively bind to the other hENT isoforms, hENT2-4 were also analyzed using the Calmodulin Target Database. I found that each isoform also contains a putative CaM binding site. Sequence alignment analysis was also performed on the region of the CaM consensus binding site in all hENT proteins (Figure – 7b). While the exact CaM binding motif of the hENT proteins is unknown, these *in silico* data demonstrate that all the human ENTs show putative CaM binding.

Figure - 7: Sequence alignment of hENTs and mENT1:

A) Sequence alignment of hENT1 and mENT1 to a number of different calmodulin binding proteins which have the 1-5-10 binding motif. Amino acids highlighted in red show the 1-5-10 positions. B) All the human ENTs were analyzed by the Calmodulin Target Database. The *in silico* data show that each of the hENT proteins has a putative calmodulin binding site, although the exact motifs are still not known.

3.2.2 CaM Alignment

To establish a putative model for CaM binding with the intracellular loop of hENT1, a model of calcium-loaded CaM bound to myosin light chain kinase from *Drosophila melanogaster* was obtained from the Protein Data Bank under accession code 2BBN. CaM is 148 amino acids in length and is highly conserved in all vertebrates and invertebrates [20]. *Drosophila* CaM has a high degree of homology to human CaM (with 2 conserved amino acid substitutions and a glutamine instead of threonine at position 143). A combination of PyMol and SWISS-MODEL were used to create a CaM/hENT1 model. Based on the sequence alignments (Figure – 7a) and analysis of the model derived by modeling of MLCK containing the hENT1 CaM binding site docked in with CaM, the 3 hydrophobic amino acids that are predicted to be involved in the binding cleft for hENT1 and CaM are Phe231, Tyr235, Leu240 (Figure 8).

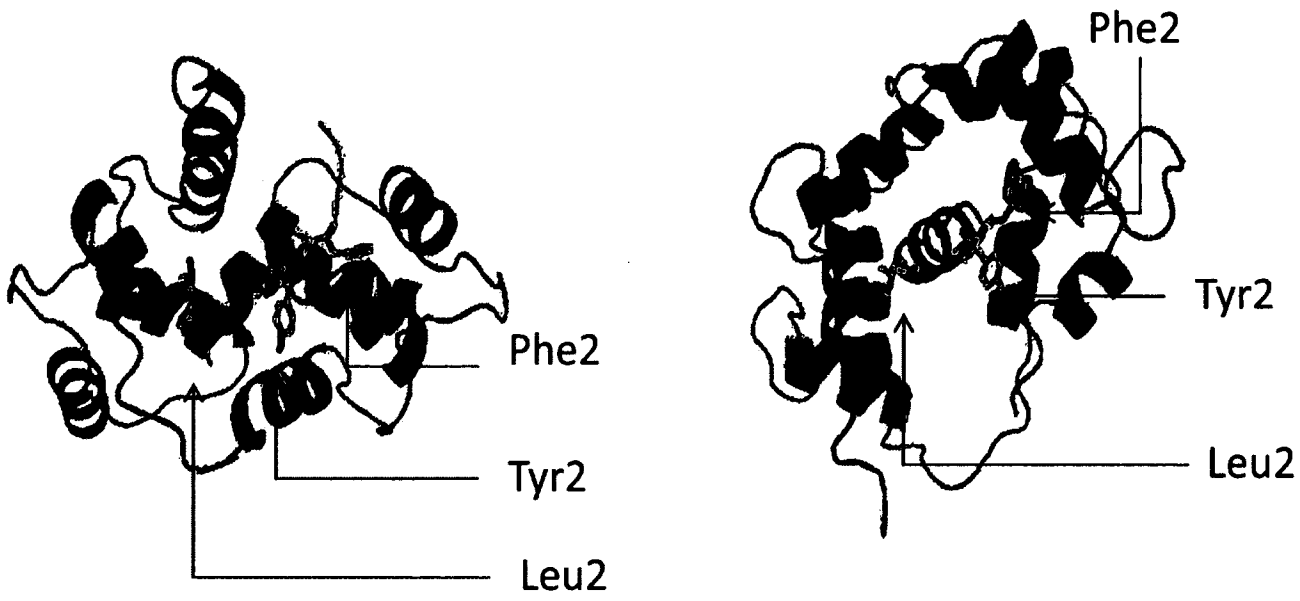

Figure - 8: Putative model of CaM-hENT1 interactions:

Putative model of CaM binding to the large intracellular loop of hENT1. The template used is of calcium loaded CaM bound to myosin light chain kinase from *Drosophila melanogaster* obtained from the PDB:2BBN. The putative hENT1 CaM binding site was threaded into the alpha helix of the myosin light chain kinase. The putative binding amino acids are highlighted in red.

3.3 NMR Spectroscopy

To test the prediction made by the *in silico* analysis of the putative ENT1-CaM binding site, and to confirm the interaction detected using MYTH, I used NMR spectroscopy to investigate whether there was a biochemical interaction between the ENT1 loop and CaM. The large intracellular loop of hENT1 and mENT1 is predominantly unstructured [89]. However, on binding, CaM is predicted to force a conformational change in the unstructured loop to an alpha-helix conformation [57]. ^{15}N-labeled CaM was titrated with ubiquitin-hENT1 and the limited amount of line broadening suggested that hENT1 is weakly binding to CaM (Figure – 10a).

However, as shown in Figure - 9, there is a large conformational change in the ENT1-loop-CaM complex in the presence of calcium, whereby >50% of the peaks shift [57]. In contrast, in the absence of calcium, there are very few shifts in peaks in the absence of calcium, suggesting that no conformational change occurs (Figure – 10a). When CaM is loaded with calcium, chemical shift changes occured providing evidence for an interaction between the hENT1-loop and CaM in the presence of calcium (Figure – 10b). The ^{15}N-labeled CaM and Ubiquitin-hENT1-loop comprise a 40kDa complex, whose spectral quality was reduced from the effects of dynamics (i.e. the proteins not holding a rigid structure). The overall complex was too large for a full structural determination [50]. To address this problem and increase resolution of the signal, thrombin was added to liberate

the ubiquitin from hENT1-loop and the histidine tag from CaM, allowing for better resolution of the peaks.

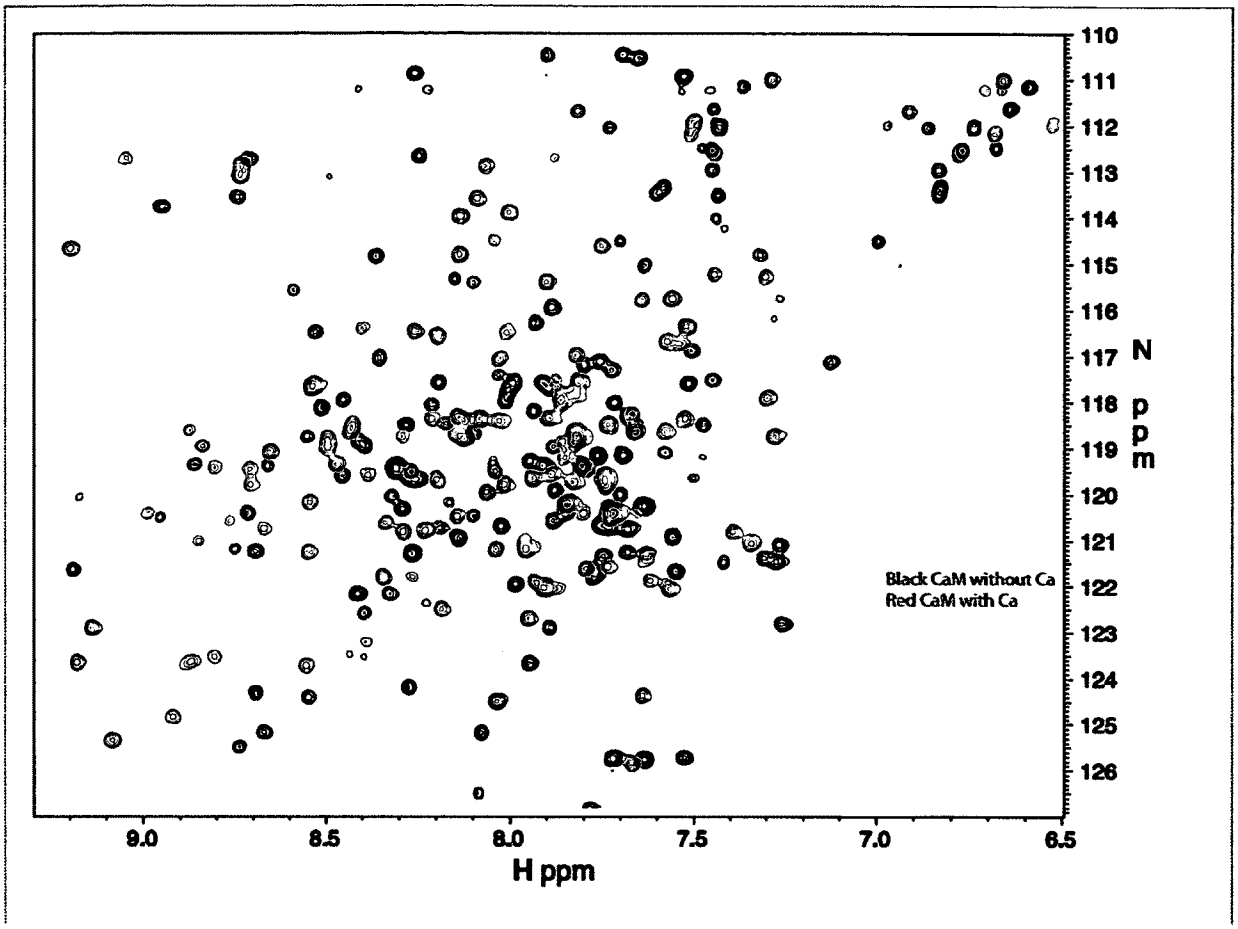

Figure - 9: The conformation of CaM changes in the presence of calcium:

HSQC of CaM in the presence (red) and absence (black) of calcium. CaM was analyzed in the absence of calcium and then loaded with 4 equivalents of calcium which leads to >50% of the peaks shifting indicating that there is a conformational change

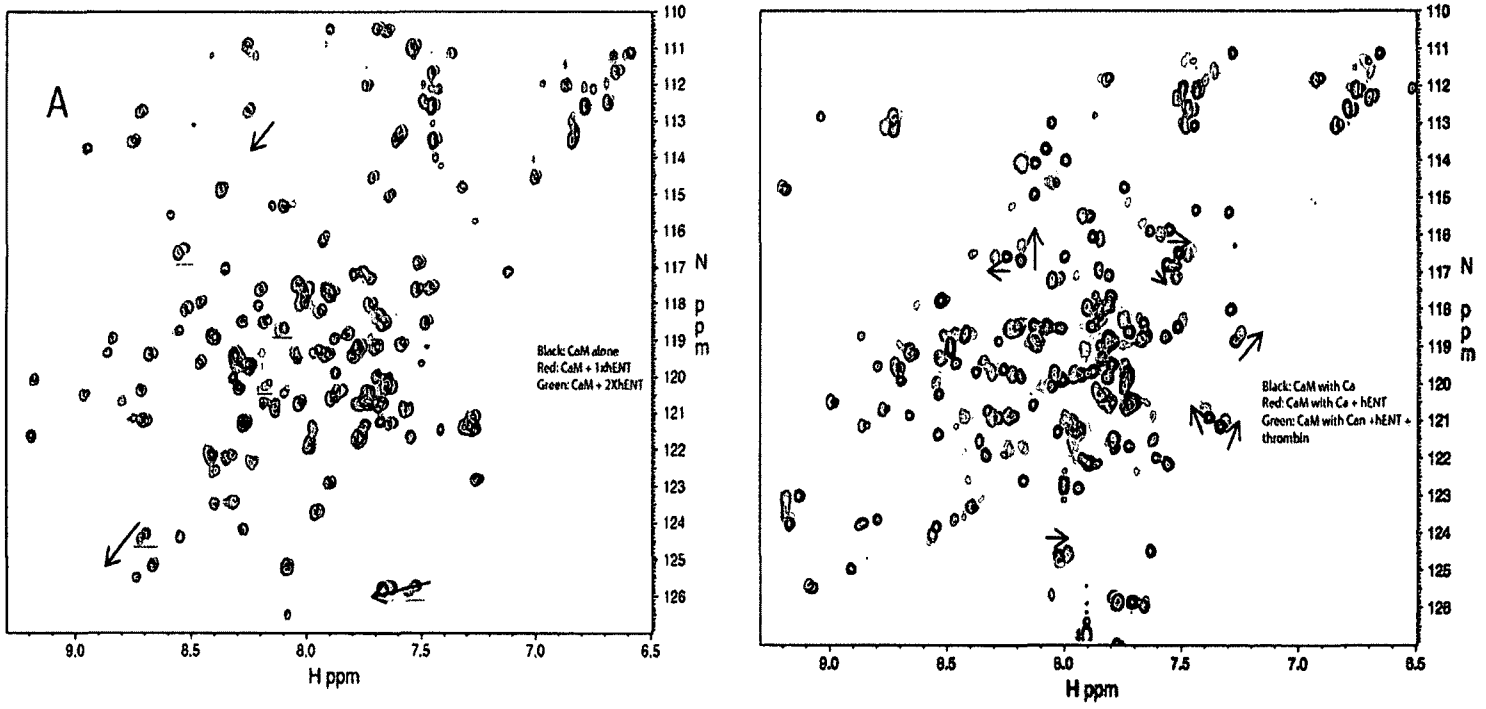

Figure - 10: NMR Analysis showing CaM-hENT1-loop interaction:

A) The green peaks show CaM as it is titrated with 2x hENT1-loop. The peaks broaden slightly, indicating that interactions are very weak. B) Comparison of peaks representing CaM loaded with calcium (black) with peaks representing CaM-hENT1-loop (red) shows a loss in signal suggesting that the construct became too large for accurate analysis. Thrombin was added to liberate ubiquitin from the structure, causing the peaks to reappear. As CaM binds to hENT1-loop the peak shift is more dramatic (green) indicating protein-protein interaction. Black arrows indicate direction of the peak shifts.

3.4 Fluorescence Anisotropy

The interaction between CaM and hENT1-loop was confirmed with NMR spectroscopy although the kinetics of the interaction were not determined. To further verify the interaction as well as determine the dissociation constant, I used fluorescence anisotropy. Relative anisotropy was measured at an excitation wavelength of 494nm and an emission wavelength at 523nm and results showed saturation allowing a binding curve to be calculated (Figure 11). These data resulted in calculation of a dissociation constant of K_d = 5.86 +/- 0.52 μM (which is considered moderate affinity) and further confirms physiologically plausible interaction between CaM and hENT1-loop. These data also confirm that the region of the CaM binding site on the large intracellular loop is as identified via the Calmodulin Target Database [125].

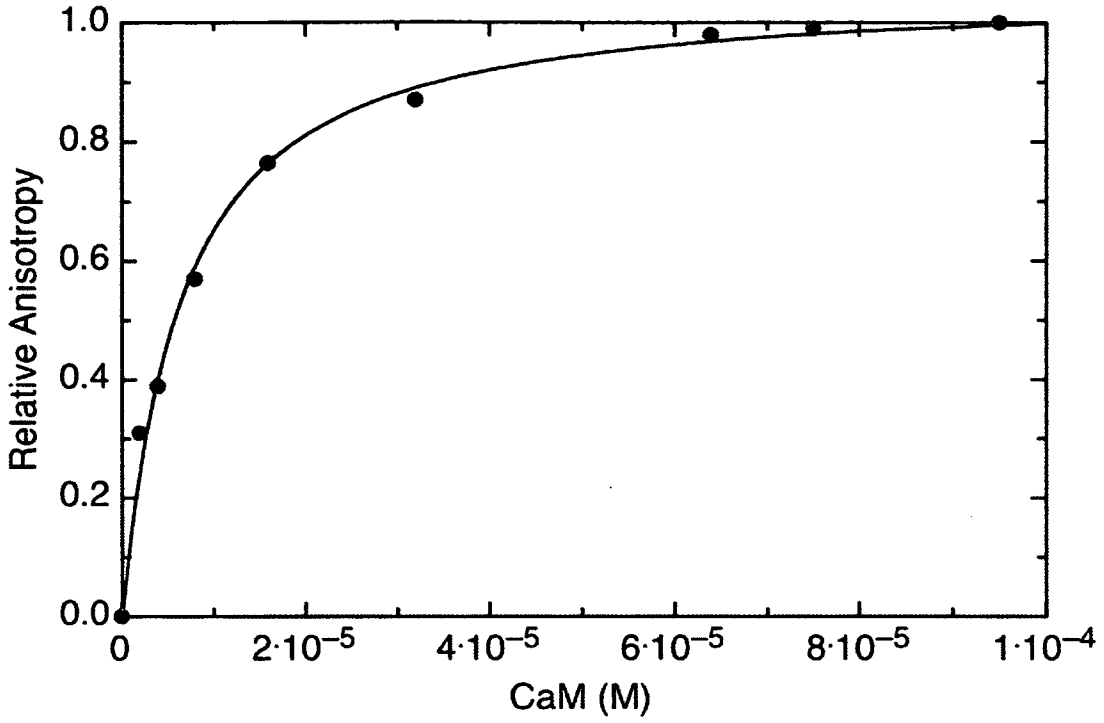

Figure - 11: Fluorescence anisotropy of CaM-hENT1-loop:

Fluorescence anisotropy graph showing the binding of calmodulin (CaM) and the fluorescently tagged hENT1-loop peptide containing the putative CaM binding site. The following curve was averaged from three runs with CaM concentrations of 0, 2, 4, 8, 16, 32, 64, 75, 95 μM, and with the fluorescently tagged peptide at 2μM, K_d = 5.86 ± 0.52 μM. (Raw data shown in Table - 2).

3.5 Determination of ENT1 phosphosites

To confirm these putative phosphosites previously identified by our laboratory, the large intracellular loops were expressed and phosphorylated *in vitro* with PKA. The protein was digested with trypsin and peptides were analyzed via multiple reaction monitoring analysis (MRM) on an Eksigent MDLC-QTRAP 4000 (AB Sciex) mass spectrometer.

Analysis of the tryptic digest of the mENT1 peptide using MRM-triggered EPI (enhanced product ion) scan revealed a peak at 1772.74 m/z corresponding to the sequence REEpSGVPGPNSPPTNR (Figure - 12), which contains serines 264 and 271. When an amino acid is phosphorylated there will be an 80 Dalton increase in its mass relative to its unphosphorylated version. MS/MS fragmentation of this peak showed that, relative to peptides of identical sequence, the 1772.74 peak was 80 Da heavier in mass then other corresponding peak, 1692.82 m/z, found via Mascot analysis. Table - 3 shows the Mascot data for the analysis of tryptic peptides. Singly-charged peptides indicate that the masses given for the amino acids show that Ser264 in mENT1 (residue 3 in the peptide) is ~80Da heavier in mass than it normally would be, which demonstrates that the peptide is phosphorylated at that specific residue.

Analysis of human ENT1-loop was more challenging because there are 6 serines in the same region of the unstructured loop compared to mENT1 (i.e. twice the number found in hENT1-loop). Repeated analysis of the hENT1 loop suggested that this region is multi-phosphorylated. Analysis of the tryptic digest

of the hENT1 peptide using MRM-triggered EPI (enhanced product ion) scan revealed a peak at 2451.09 m/z corresponding to the sequence AGKEESGVpSVSNSQPTNESHSIK (Figure - 13), which contains Ser266, Ser269, Ser271,Ser273, Ser279, Ser281. The following tryptic peptide was 80 Da heavier in mass at Ser269 (residue 9 in the peptide); Table - 4 shows the Mascot data for the tryptic peptide, indicating an 80 Da increase residue 9. The same EPI scan that revealed the 2451.09 m/z peak also revealed a peak at 2194.94 m/z corresponding to the sequence EEpSGVSVSNSQPTNESHSIK (Figure - 14). This tryptic peptide also shows an 80 Da increase in Ser266 (residue 3 in the peptide) as shown in the Mascot data in Table - 5. Initial scans of hENT1 demonstrated observed peak shifts from 2371.12 m/z to 2451.09 m/z for serine 269 and a shift from 2114.97 m/z to 2194.94 m/z for serine 266, indicating that hENT1 is multi-phosphorylated.

A second run using MRM-triggered EPI scan of hENT1 also showed and reconfirmed phosphorylation of hENT1. MS-MS fragmentation of the tryptic peptide, EESGVSVpSNSQPTNESHSIK, revealed a peak at 2194.94 m/z, which suggested that Ser271 (residue 8) in this peptide is phosphorylated, Table – 6 shows the Mascot data for the tryptic peptide, indicating an 80Da increase at residue 8. The EPI spectrum also showed evidence through manual search of the peaks that three of the four N-terminal positions, Ser266, Ser271, Ser273 (residue, 3, 8, 10 respectively) and one of the two C-terminal serines, Ser279/Ser281 (residue 16/18 respectively) is also phosphorylated (Figure - 15).

A comparison of the phosphosites for mENT1 and hENT1 show that only the first phosphorylated serine is in the same region (Figure – 16).

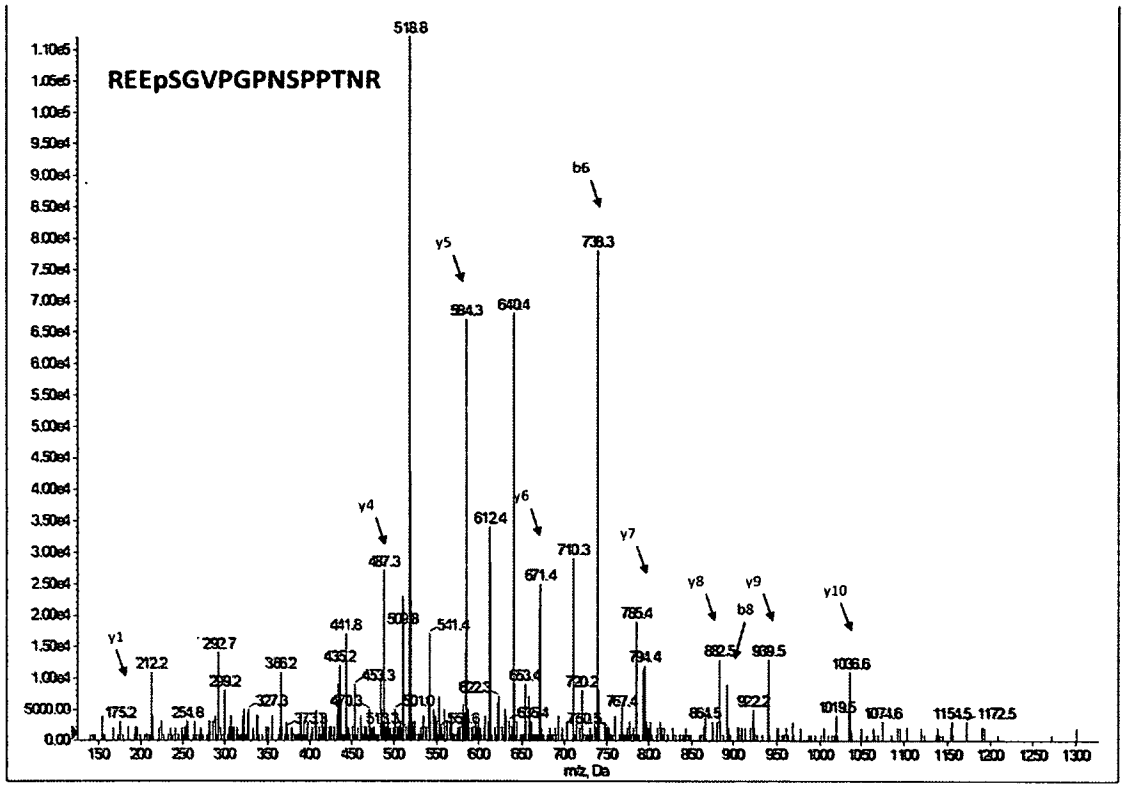

Figure - 12: MS-MS scan of mENT1 showing Serine 264 phosphosite:

Mass spectrometry analysis of mENT1 large intracellular loop. This is a representative image of a tryptic digest of PKA treated mENT1-loop resulting in a peptide REESGVPGPNSPPTNR. The spectrum indicates that residue 4 in the peptide is phosphorylated. The red and the green arrows indicate major ions in the y/b-series of the peptide. Mascot data for this spectrum is shown in Table - 2

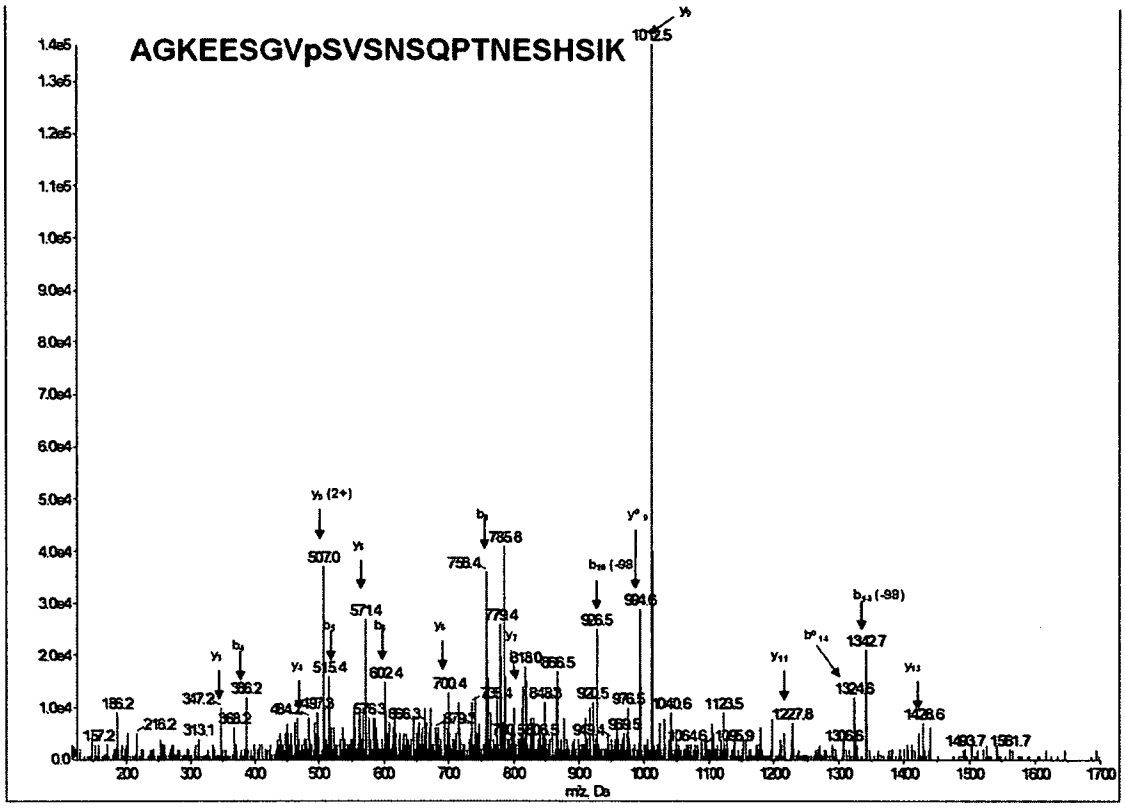

Figure - 13: MS-MS scan of hENT1-loop showing Serine 269 phosphosite:

Mass spectrometry analysis of hENT1 large intracellular loop. This is a representative image is of a tryptic digest of PKA treated hENT1-loop resulting in a peptide AGKEESGVpSVSNSQPTNESHSIK. The spectrum indicates that residue 9 in the peptide is phosphorylated. The red and the green arrows indicate major ions in the y/b-series of the peptide. Mascot data for this spectrum is shown in Table - 3.

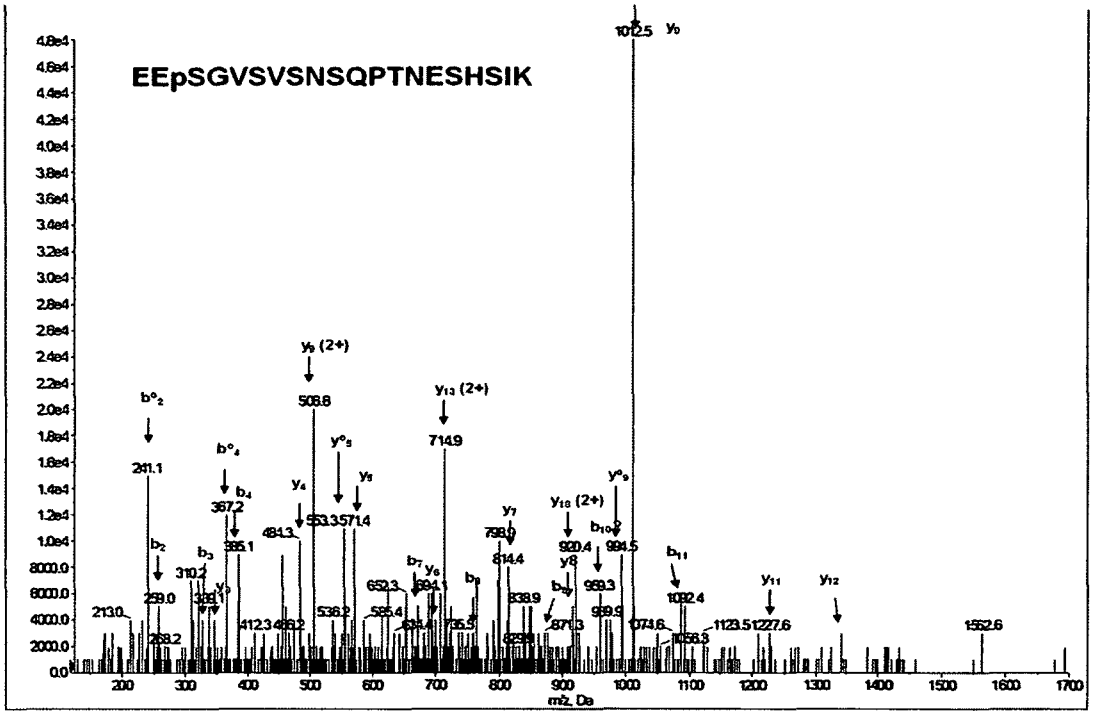

Figure - 14: MS-MS scan of hENT1 showing Serine 266 phosphosite:

Mass spectrometry analysis of hENT1 large intracellular loop. This is a representative image is of a tryptic digest of PKA treated hENT1-loop resulting in a peptide AGKEESGVpSVSNSQPTNESHSIK. The spectrum indicates that residue 3 in the peptide is phosphorylated. The red and the green arrows indicate major ions in the y/b-series of the peptide. Mascot data for this spectrum is shown in Table – 4.

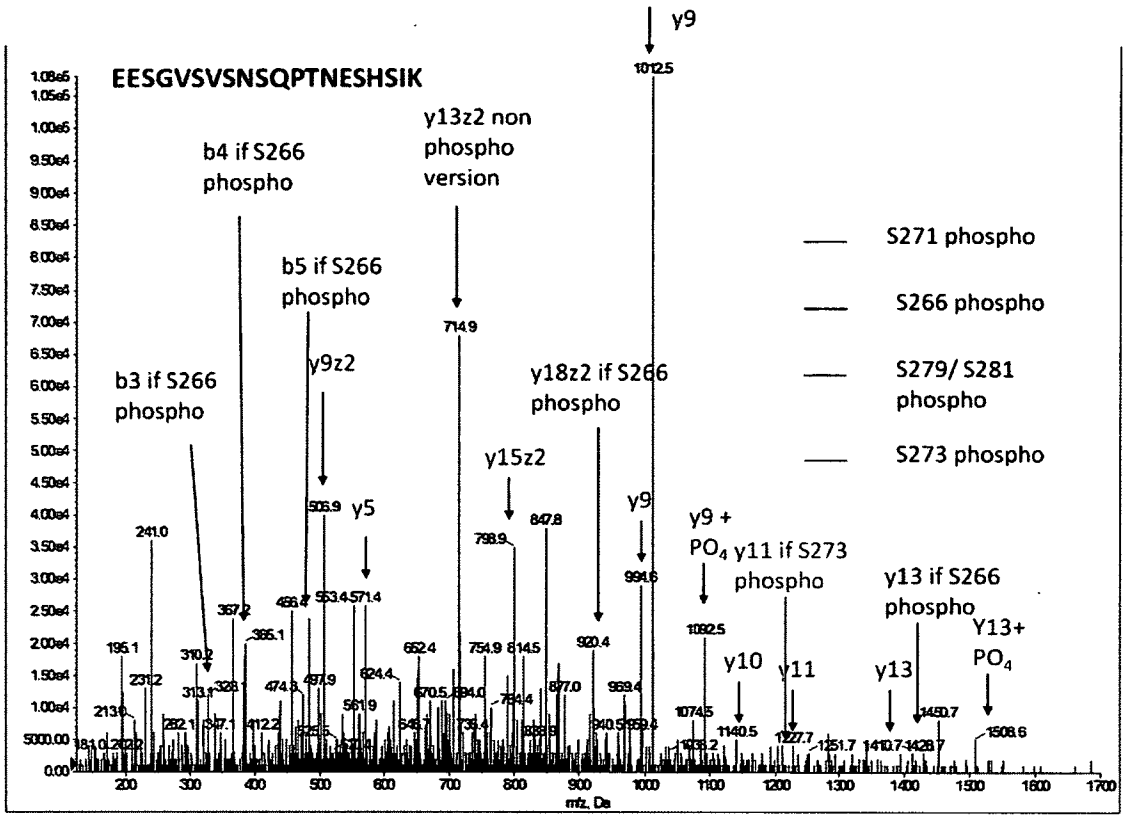

Figure - 15: MS-MS scan of hENT1 showing Serine 266, 271, 273, 279/281 Phosphosites:

Mass spectrometry analysis of hENT1 large intracellular loop. This is a representative image is of a tryptic digest of PKA treated hENT1-loop resulting in a peptide EESGVSVSNSQPTNESHSIK. An EPI scan of the peptide indicated that 3 of the N-terminal serines as well as one of the two C-terminal serines have been phosphorylated in vitro. Black arrows indicate that residue 3 is phosphorylated, red arrows with residue 8, 10 with green arrows, and either residue 16/18 with purple arrows. Residue 6 on this peptide was previously shown to be phosphorylated with an MS-MS scan of AGKEESGVpSVSNSQPTNESHSIK (Shown as residue 9) in figure-13.

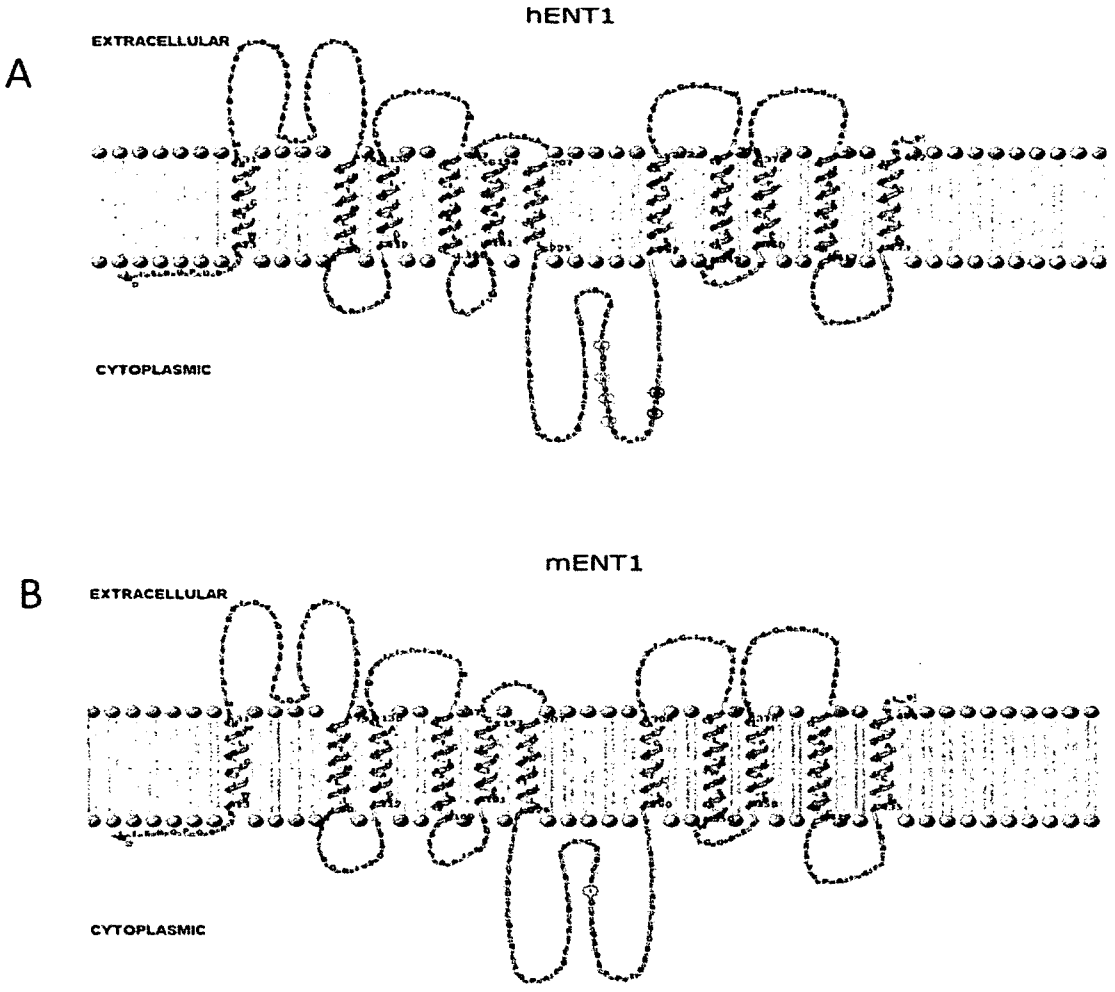

Figure - 16: hENT1 and mENT1 phosphosites:

The proposed two-dimensional topologies of hENT1 and mENT1 with the confirmed phosphosites shown in red. A) hENT1: Ser266, Ser269, Ser271, Ser273, Ser279/Ser281 were confirmed as being phosphorylated by PKA *in-vitro*. Ser279 and Ser281 are highlighted in blue, since it is not known which one of the two is phosphorylated. B) mENT1: Ser264 was the only serine in the large intracellular loop that was shown to be phosphorylated by PKA *in-vitro*.

Chapter 4: Discussion

The primary objective of my thesis was to identify novel ENT1 interacting partners. Upon completion of this objective, I confirmed one of the interactions with hENT1 via subsequent biochemical screens, and identified novel phosphosites *in vitro* in both proteins. Through MYTH screening of mENT1, a putative protein interactome was obtained from the mouse genome with one confirmed interacting partner confirmed through functional analyses. Since there are currently no reports in the literature of any interacting partners of hENT1 or mENT1, this result is significant. Of the six confirmed interacting partners, calmodulin (CaM) was chosen for further validation via NMR under two conditions; in the presence and absence of calcium. Fluorescence anisotropy was used to determine a dissociation constant for the CaM-ENT1 interaction. Subsequent analyses were performed using mass spectrometry to validate whether or not the large intracellular loop of hENT1 and mENT1 are phosphorylated *in vitro*.

4.1 CaM a novel hENT1 interactor

My molecular model suggests that the ENT1 loop is largely unstructured and likely to be free floating in the cytoplasm of the cell. Interaction with CaM results in the loop gaining some structure [57] as has been observed with other CaM binding proteins. Interestingly, CaM tends to bind to large intracellular loops of integral membrane proteins. For instance, Zhou et al. (2007) identified a CaM

binding site on Connexin43 (Cx43), which is a gap junction protein. They discovered that CaM binds between residues 136-158 in a Ca2+ dependent manner, and similar to hENT1 and CaM binding it occurred at a 1:1 binding ratio [127]. The regulation that CaM binding exerts on Cx43 is that it induces a structural change, such that the protein becomes less permeable [127]. Zhou *et al.* (2009) also showed that CaM binds to Connexin44 (Cx44) in its only intracellular loop region at residues 129-150. Similar to CaM binding to Cx43, it is also Ca^{2+} dependent as well as through circular dichroism spectroscopy, the intracellular loop gains secondary and tertiary structure [128]. Both proteins are regulated by Ca^{2+} levels in the cell, suggesting that hENT1 is also likely regulated in a Ca^{2+}- CaM dependent manner, whereby CaM binding can cause a structural change in the large intracellular loop of hENT1, possibly making the protein more or less permeable to nucleosides. Iwamoto *et al.* (2010) showed that ATP-binding cassette transporter A1 (ABCA1) binds to CaM in a Ca^{2+}-dependent manner via the cytoplasmic loop of ABCA1 at residues 1245-1257 [56]. ABCA1 is a membrane protein which facilitates in the transport of cholesterol and phospholipids into the cell from the production of high density lipoproteins (HDL) [56]. These researchers showed that binding of CaM to ABCA1 protected the protein from proteolysis by calpain. CaM is able to offer this protection because the calpain cleavage site and the CaM binding site share a similar region on the intracellular loop of ABCA1 [56]. CaM binding may also offer similar protection to hENT1, possibly against proteases.

The identification of CaM and hENT1 as novel interactors in the presence of calcium suggests that this ion has an important role in the regulation of hENT1. CaM can also bind to other proteins in the absence of Ca^{2+}, such as Myosin V [79]. It has been shown with other transporters that CaM plays a role in the regulation of some membrane transporters but there have been few any papers that have shown a correlation between Ca^{2+} flux and the regulation of nucleoside transport across the cell membrane. The overall role of Ca^{2+} in the regulation of hENT1 and other nucleoside transporters needs to be more thoroughly investigated especially since there is an enormous body of literature on the regulation of membrane proteins by calcium [56, 124, 127, 128]. Membrane proteins are also responsible for the flux of calcium into cells and across membranes [28] therefore Ca^{2+} flux and regulation of membrane proteins, such as the ENTs, would appear to be a plausible, but almost completely overlooked, physiological phenomenon.

One recent small insight in the relationship between ENTs and Ca^{2+}, was described in 2009 by Zamzow *et al.* [126]. This group demonstrated that an increase in Ca^{2+} in the cell through activation of NMDA receptors led to activation of calmodulin kinase II (CaMKII), which is regulated by interactions with calmodulin. The group reported that CaMKII in turn then appears to modulate nucleoside transport via rat ENT2 [126]. These data support a role for CaM and Ca^{2+}-dependent regulation of the ENTs although they do not describe and underlying mechanism as I have presented in this thesis. Another paper published in 2010 by Knight *et al.* [66] showed that hypomorphic mutations in

Drosophila ENT2 result in a change in the flux of Ca^{2+} in the cell [66] – taken together these studies provide evidence for a relationship between ENT transporters and Ca^{2+}. I have extended these findings with mechanistic data.

Binding of CaM to the large unstructured loop of hENT1 causes a structural change in this region which may results in subtle or substantial changes in the entire hENT1 structure, including the possibility of the opening or closing of a pore complex as described above with Cx43 and Cx44 [127, 128]. A pore complex has been proposed for the ENT proteins. Arastu-Kapur et al. (2005) showed *Leishmania donovanii* nucleoside transporter (LdNT2) that out of the 11 TM domains of ENT proteins, their proposed tertiary structure showed that TM 1, 2, 4, 5, 8, 10, 11 form a pore complex [4]. Alterations in the overall conformation of the large intracellular loop may result in a "ripple" effect, which alters the interactions of TM domains contributing to the pore and thus affecting substrate translocation. Therefore, a three dimensional structure of hENT1 is needed for us to answer many of the unknown questions such as how substrate translocation occurs and if the TM domains contribute to a pore.

CaM binding could also regulate phosphorylation by recruiting CaMKII, as suggested by Zamzow *et al* (2009) [126]. Our data show that the hENT1 phosphosites are in proximity of, but not within, the CaM binding site. Dahl *et al.* (2004) demonstrate that the structural or conformational changes in the intracellular loop (between TM8 and TM9) of the cation antiporter NhaA lead to alteration of the positions of TM4, 5 and 11, which open up the pore in the protein

[26]. While changes in the intracellular loop of NhaA are dependent on charge, conformational changes in the ENT loop as a consequence of interaction with CaM could possibly open or close a proposed pore "structure" [26].

4.2 Calmodulin: a weak interacting partner

CaM binding can happen at a wide range of affinities depending on the specific binding motif. IQ motifs in the myosin-I isoform (Myo1b), which binds to CaM, with a K_d ranging from 0.2 μM to 5 μM [72].

My results suggest that ENT1-CaM interactions have an affinity of K_d = 5.86 ± 0.52 μM, which is a relatively moderate interaction as would be expected given that many protein-protein interactions are necessarily transient and are therefore typically weak interactions. Weak or moderate interactions can be required for either rapid assembly of proteins, dissociation of protein complexes, or for signal transduction [82, 112]. Because CaM binding to hENT1 is moderately weak, it likely allows for rapid dissociation in the event of changes in local Ca^{2+} levels. This rapid dissociation of a CaM interactor was observed by Nguyen and Higuchi (2005) who showed that CaM rapidly dissociates from Myosin V arising from temporary bursts of Ca^{2+} in the cell [79]. Although CaM has been identified as the first interacting partner for ENT1, using MYTH, NMR, and fluorescence anisotropy, the physiological relevance of this interaction is still not understood. Given the diversity of roles that CaM is already known to be involved in, it is possible that it interacts with ENT1 to regulate or facilitate

recruitment of other proteins for phosphorylation, to modulate trafficking of the protein within the cell for recycling, or to regulate the transport activity or substrate preference/affinity.

4.3 Other mENT1 Interactions Confirmed Through MYTH

The MYTH assays performed also identified other putative interactors that were validated through bait dependency screens (Figure - 17). While only one of the interacting partners was confirmed outside of a MYTH system, the MYTH screen also identified GPI, TUBB, DnaJ, MTPN and Gpbar1.

While none of the remaining putative interacting partners have been further validated, proteins such as DnaJ (Hsp40), which helps with the folding or unfolding of many proteins could possibly have a role in facilitating the final 3-dimensional shape of mENT1 as it makes it way to the cell membrane. While large protein structures such as TUBB, can be used to anchor mENT1 into the cell membrane. One possible relationship between myotrophin (MTPN) and ENT1 is that proteins such as MTPN have been shown to increase protein synthesis and stimulate cellular hypertrophy, while uptake of adenosine into the cell has been shown to inhibit cellular hypertrophy [3, 28]; hinting that these two proteins might play a role with each other for cell growth and protein synthesis. Further investigations into these putative interactors would provide enormous insight into the ENT1 interactome.

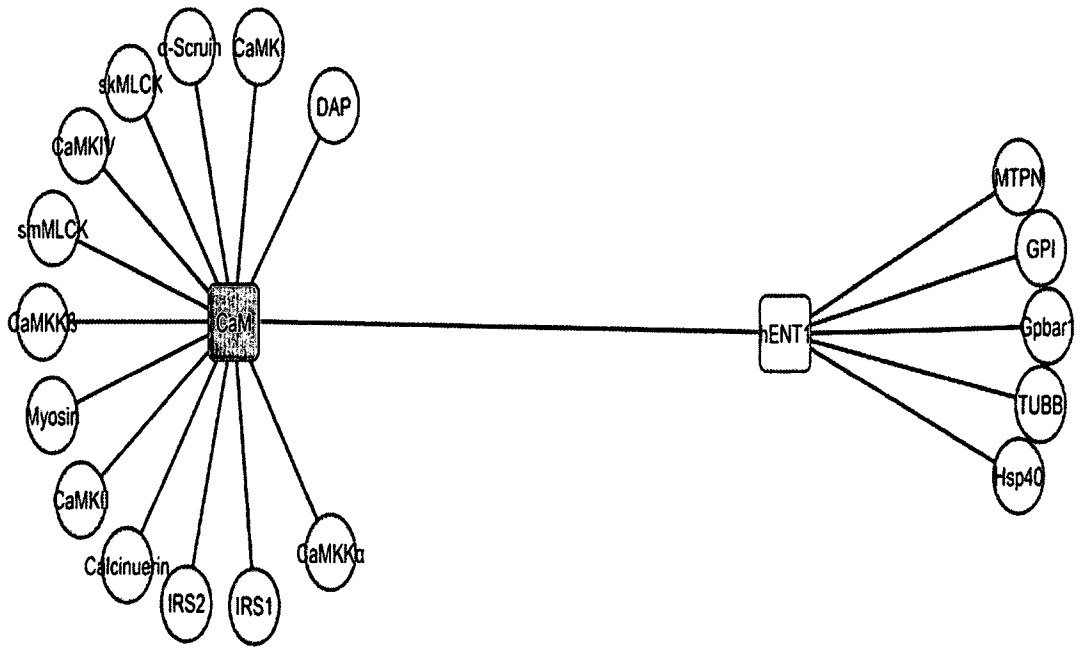

Figure - 17: CaM and putative hENT1 interactome:

The hENT interactome identified with MYTH. The interacting partners of hENT1 are shown via the nodes linked to hENT1, subsequently the same is shown for just a few of the interacting partners of calmodulin [125]. The red edge, linking hENT1 and CaM is the only interacting partner that was subsequently confirmed to interact via NMR, and anisotropy to further confirm that it is a true interacting partner outside of MYTH. Blue edges are interactions with hENT1 that have yet to be confirmed outside of a MYTH system.

4.4 ENT1 phosphorylation

There is currently only one published report demonstrating that human or murine ENT1 is directly phosphorylated [90]. The specific phosphorylation sites remain unknown. The identification of specific phosphosites within the large intracellular loops of both h/mENT1 was a major aim of this thesis.

While there have been many reports of kinase-dependent regulation of ENTs, no link has been established between phosphorylation and function. For example, Calotti *et al.* (2008) proposed that PKC regulates hENT1 transport activity and nucleoside uptake [62]. IL-4 is a survival signal in CLL cells that has been shown to bestow resistance to nucleoside analogs. CLL cells treated with IL-4 showed increased hENT1 mRNA expression via PKC activation [62].

The data presented in this thesis clearly show that the large intracellular loops of mENT1 and hENT1 are directly phosphorylated *in vitro* by PKA; also, that the hENT1-loop can be phosphorylated at multiple sites. Our data for the mENT1-loop suggests that Ser264 is phosphorylated by PKA *in vitro*, Further kinase assays need to be performed to conclusively show that mENT1, and unlike its human homolog is only phosphorylated at one site between TM domains 6 and 7.

When a protein has the ability to be phosphorylated in multiple locations, the order which phosphorylation occurs is important. This is because the order in which kinases and phosphatases add and remove phosphate groups is dictated

by the quantity of phosphosites that exist on the protein as well as its surrounding consensus sequences [99]. Having determined that the hENT1-loop is capable of being phosphorylated at multiple sites, it now becomes important for our understanding of hENT1 to decipher the order in which phosphorylation takes place. Moreover, since human and murine ENT1 share 78% amino acid sequence homology, there is a possibility that perhaps mENT1 has multiple phosphosites on the large intracellular loop as well.

Multi-site phosphorylation of membrane proteins has been observed in the insulin receptor. There are at least five tyrosines in the β-subunit of the receptor that are phosphorylated [62]. When three of these tyrosines (1146, 1150, 1151) are phosphorylated, the kinase is additionally activated toward exogenous substrates [62]. This is important for signal transduction, since the kinase remains active as long as dephosphorylation does not take place [62].

Phosphorylation of membrane proteins can also lead to internalization. Jayanthi et al. (2006) showed that when the norepinephrine transporter (NET) is phosphorylated at Thr258 and Ser259 by PKC, it is internalized [58]. Similarly, a correlation exists for DAT, whereby N-terminal serines were shown to be phosphorylated by PKC [41], and recycling of DAT from the plasma membrane was shown to be mediated by activation of PKC [27]. Therefore, phosphorylation of ENT1 may play a role in the internalization and trafficking of the protein throughout the cell.

My studies of ENT1 phosphorylation have shown that this mode of regulation occurs *in vitro* and that regulation of phosphorylation in hENT1 is far more complicated than the initial data had suggested. In turn, these data clearly warrant further study to determine whether phosphorylation of ENT1 happens *in vivo* and if other kinases are involved. In turn, since phosphorylation and dephosphorylation are powerful mechanisms for cells to regulate their internal cellular machinery, elucidating further information about the dynamics of ENT1 phosphorylation will strengthen our understanding of its place in biological pathways.

A little over a decade has passed since hENT1 has been originally cloned [47]. Since that time, identification of its binding partners has been largely ignored because of the difficulty of biochemical analysis of these challenging membrane proteins. The identification of calmodulin in this thesis serves as a springboard for the identification of additional partners. The ultimate objective of this thesis and studies extending from it is a complete understanding hENT1's structural and functional attributes.

Chapter 5: Future Directions

In this study I uncovered mENT1 interactors using MYTH technology and validated CaM interactions with hENT1 through NMR and fluorescence anisotropy. Further work is necessary to identify whether the remaining partners identified also interact with hENT1 or mENT1 outside of a MYTH system. I have demonstrated that methods such as NMR and fluorescence anisotropy provide detailed information regarding the binding characteristics of ENT1. In the future, it may be beneficial to explore other protein detection platforms such as bimolecular fluorescence complementation and phage display

Using peptides, I have identified a site in ENT1 that is bound tightly by calmodulin. A logical extension of this work is to perform a mutagenesis study.. These study would further our understanding of the CaM-hENT1 interaction and give insight to any downstream regulation or signal pathways that may occur via CaM binding with hENT1. An alternative approach to understanding the structure and function of ENT1 would be to elucidate the three dimensional structure of the complex, either by NMR or X-ray crystallography. If co-localization assays show proximity of CaM to hENT1 *in vivo* then FRET analysis can also be performed to see CaM and hENT1 interaction in real-time, as well as any other hENT1 interacting partners that may be identified in the future.

The kinase assays coupled with LC- MRM mass spectrometry identified phosphosites on the large intracellular loops of both mENT1 and hENT1 *in vitro*. Experiments to detect these phosphosites on the full-length protein are being

planned, as well as analysis of the endogenous protein. If identified *in vivo*, site-directed mutagenesis experiments can be performed to elucidate the functional significance of these phosphosites, especially with hENT1 since it is multiphosphorylated.

References

1. Aly, A.S.I., Downie, M.J., Mamoun, C.B., Kappe, S.H.I. (2010). Subpatent infection with nucleoside transporter 1-deficient *Plasmodium* blood stage parasites confers. Cell Microbiol. 12(7): 930-938.

2. Anderson, C. M., Baldwin, S a, Young, J D, Cass, C E, & Parkinson, F E. (1999). Distribution of mRNA encoding a nitrobenzylthioinosine-insensitive nucleoside transporter (ENT2) in rat brain. Brain ResMol Brain Res. 70(2): 293-7.

3. Anderson, K. M., Berrebi-Bertrand, I., Kirkpatrick, R. B., McQueney, M. S., Underwood, D. C., Rouanet, S., & Chabot-Fletcher, M. (1999). cDNA sequence and characterization of the gene that encodes human myotrophin/V-1 protein, a mediator of cardiac hypertrophy. J Mol Cell Cardiol. 31(4): 705-719.

4. Arastu-Kapur, S., Arendt, C.S., Purnat, T., Carter, N. S., Ullman, B. (2005). Second-site suppression of a nonfunctional mutation within the *Leishmania donovani* inosine-guanosine transporter. J Biol Chem. 280(3): 2213-2219.

5. Aymerich, I., Foufelle, F., Ferre, P., Casado, F.J., Pastor-Anglada, M. (2006). Extracellular adenosine activates AMP-dependent protein kinase (AMPK). J Cell Sci. 119: 1612-1621.

6. Baldwin, S.A., Mackey, J.R., Cass, C.E., Young, J.D. (1999). Nucleoside transporters: molecular biology and implications for therapeutic development. Mol Med Today. 5(5): 216-24.

7. Baldwin, S. A., Beal, P. R., Yao, S. Y. M., King, A. E., Cass, C.E., Young, J.D. (2004). The equilibrative nucleoside transporter family, SLC29. Pflügers Archiv. 447(5): 735-43.

8. Baldwin, S.A., Yao, S.Y.M., Hyde, R.J., Ng, A.M.L., Foppolo, S., Barnes, K., Ritzel, M.W.L., Cass. C.E., Young, J.D. (2005). Functional characterization of novel human and mouse equilibrative nucleoside transporters (hENT3 and mENT3) located in intracellular membranes. J Biol Chem, 280(16): 15880-7.

9. Balnave, K., Neill, J.D., Russell, C.J., Harron, D.W.G., Leahey, W.J., Shanks, R.G. (1981). Observations on The Efficacy and Pharmacokinetics of Betaxolol (SL 75212), A Cardioselective β-Adrenoceptor Blocking Drug. Br J Clin Pharac. 11: 171-180.

10. Barford, D., Das, A.K., Egloff, M.P. (1998). The structure and mechanism of protein phosphatases: insights into catalysis and regulation. Annu Rev Biophys Biomol Struct. 27: 133-64.

11. Barnes, K., Dobrzynski, H., Foppolo, S., Beal, P.R., Ismat, F., Scullion, E.R., Sun, L., Tellez, J., Rtizel, M.W.L., Claycomb W.C., Cass. C.E., Young. J.D., Billeter-Clark, R., Boyett, M.R., Baldwin, S.A. (2006). Distribution and functional characterization of equilibrative nucleoside transporter-4, a novel cardiac adenosine transporter activated at acidic pH. Circ Res. 99(5): 510-9.

12. Betcher, D. L., Burnham, N. (1990). Cytarabine. J Pediatr Oncol Nurs. 7(4): 154-157.

13. Brymora, A., Valova, V.A., Robinson, P.J. (2004). Protein-protein interactions identified by pull-down experiments and mass spectrometry. Curr Protoc Cell Biol Chapter 17: Unit 17.5.

14. Buijs, J., and Franklin, G.C. (2005). SPR-MS in functional proteomics. Brief Funct Genomics Proteomic. 4(1): 39-47.

15. Butler, V.P., Beiser, S.M., Erlanger, B.F., Tanenbaum, S.W., Cohen, S., Bendich, A. (1962). Purine-specific antibodies which react with deoxyribonucleic acid (DNA). Proc Natl Acad Sci U S A. 15(48): 1597-602.

16. Canet, D., Doering, K., Dobson, C.M., Dupont, Y. (2001). High-sensitivity fluorescence anisotropy detection of protein-folding events: application to alpha-lactalbumin. Biophys J. 80(4): 1996-2003.

17. Cerecedo, L.R. (1927). Studies on the physiology of pyrimidines. J Biol Chem. 75: 661-670.

18. Chang, C., Stewart, R.C. (1998). Update on Signal Transduction The Two-Component System 1 Regulation of Diverse Signaling Pathways in Prokaryotes and Eukaryotes. Plant Physiol. 117: 723-731.

19. Chen, D.C., Yang, B.C., Kuo, T.T. (1992). Short communications One-step transformation of yeast in stationary phase. Curr Genet. 21: 83-84.

20. Chien, Y.H., and Dawid, I.B. (1984). Isolation and characterization of calmodulin genes from *Xenopus laevis*. Mol Cell Biol. 4(3):507-13.

21. Clark, S.M., Konermann, L. (2004). Determination of ligand-protein dissociation constants by electrospray mass spectrometry-based diffusion measurements. Anal Chem. 76(23), 7077-7083.

22. Clercq, E.D., Field, H.J. (2006). Antiviral prodrugs – the development of successful prodrug strategies for antiviral chemotherapy. Br J Pharmacol. 147: 1-11

23. Cole, P., Shen, K., Qiao, Y., Wang, D. (2003). Protein tyrosine kinases Src and Csk: a tail's tale. Curr Opin Chem Biol. 7(5): 580-585.

24. Cozzone, A.J. (1988). Protein phosphorylation in prokaryotes. Annu Rev Microbiol. 42: 97-125.

25. Crawford, C. R., Patel, D. H., Naeve, C., & Belt, J. A. (1998). Cloning of the human equilibrative, nitrobenzylmercaptopurine riboside (NBMPR)-insensitive nucleoside transporter ei by functional expression in a transport-deficient cell line. J. Biol. Chem. 273(9): 5288-93.

26. Dahl, S.G., Sylte, I., Ravna, A.W. (2004). Structures and models of transporter proteins. J Pharmacol Exp Ther. 309(3): 853-860.

27. Daniels, G.M. and Amara, S.G. (1999). Regulated trafficking of the human dopamine transporter. J Biol Chem. 274(50): 35794-35801.

28. Dipolo, R. And Beauge, L. (2006). Sodium/calcium exchanger: influence of metabolic regulation on ion carrier interactions. Physiol Rev. 86: 155-203.

29. Drury, A.N., Gyorgyi, A.S. (1929). The physiological activity of adenine compounds with especial reference to their action upon the mammalian heart. J Physiol. 68(3): 213-37.

30. Dukhovich, F.S., Gorbatova, E.N., Darkhovskii, M.B., Kurochkin, V.K. (2002). Relationship between the dissociation constant and the lifetime for complexes of biologically active substances with receptors and enzymes. Pharm Chem J. 36(5): 248-254.

31. Dunwiddie, Thomas V, & Masino, S. A. (2001). The role and regulation of adenosine in the central nervous system. Annu Rev Neurosci: 31-55.

32. Dyson, H.J., and Wright, P.E. (2002). Coupling of folding and binding for unstructured proteins. Curr Opin Struct Biol. 12(1): 54-60.

33. Elion, B., Carolina, N., Park, R.T. (1982). Mechanism of action and selectivity of acyclovir. Am J Med. 73: 7-13.

34. Engel, A., and Gaub, H.E. (2005). Structure and mechanics of membrane proteins. Mol Pharmacol. 68(5): 1397-1407.

35. Engel, K., and Wang, J. (2005). Interaction of organic cations with a newly identified plasma membrane monoamine transporter. Mol Pharm. 68(5): 1397-1407.

36. Fan, J-Y., Cui, Z-Q., Wei, H-P., Zhang, Z-P., Zhou, Y-F., Wang, Y-P., Zhang, X-E. (2008). Split mCherry as a new red bimolecular fluorescence complementation system for visualizing protein – protein interactions in living cells. Biochem Biophys Res Commun. 367: 47-53.

37. Felipe, A., Valdes, R., Santo. B.D., Lloberas, J., Casado, J., Pastor-Anglada, M. (1998). Na^+-dependent nucleoside transport in liver: twoo different isoforms from the same gene family are expressed in liver cells. Biochem J. 330: 997-1001.

38. Fernández-Veledo S, Huber-Ruano I, Aymerich I, Duflot S, Casado FJ, Pastor-Anglada M. (2006). Bile acids alter the subcellular localization of CNT2 (concentrative nucleoside cotransporter) and increase CNT2-related transport activity in liver parenchymal cells. Biochem J. 395: 337–344

39. Fetchko, M., and Stagljar, I. (2003). Application of the split-ubiquitin membrane yeast two-hybrid system to investigate membrane protein interactions. Methods. 32(4): 349-62.

40. Foster, J D., Pananusorn, B., Vaughan R.A. (2002). Dopamine transporters are phosphorylated on N-terminal serines in rat striatum. J Biol Chem. 277(28): 25178-25186.

41. Freeman-Cook, K.D., Autry, C., Borzillo, G., Gordon, D., Barbacci-Tobin, E., Bernardo, V., Briere, D., Clark, T., Corbett, N., Jakubczak, J., Kakar, S., Knauth, E., Lippa, B., Luzzio, M.J., Mansour, M., Martinelli, G., Marx, M., Nelson, K., Pandit, J., Rajamohan, F., Robinson, S., Subramanyam, S., Wei, L., Wythes, M., Morris, J. (2010). Design of selective, ATP-competitive inhibitors of Akt. J Med Chem. 53(12): 4615-22.

42. Galamarini, M.C., Almarini, G., Larke, M.L.C., Alette, N.F., Uisieux, A.P., Ackey, J.R.M., Umontet, C.D. (2002). Expression of a non-functional P53 affects the sensitivity of cancer cells to gemcitabine. Int J Cancer. 97: 439 - 445.

43. Gegelashvili, G. and Schousboe, A. (1997). High affinity glutamate transporters: regulation of expression and activity. Mol Pharmacol. 52: 6-15.

44. Gietz, R. D. and R. A. Woods. 2002. Transformation of yeast by lithium acetate/single-stranded carrier DNA/polyethylene glycol method. Methods Enzymol. 350:87-96.

45. Gray, J. H., Owen, R. P., Giacomini, K. M. (2004). The concentrative nucleoside transporter family, SLC28. Pflügers Archiv : Eur J Physiology. 447(5): 728-34.

46. Grden M, Podgorska M, Kocbuch K, Rzepko R, Szutowicz A, Pawelczyk T. (2008). High glucose supresses expression of equilibrative nucleoside transporter 1 (ENT1) in rat cardiac fibroblasts through a mechanism dependent on PKC-ζ and MAP kinases. J Cell Physiol. 215: 151 – 160

47. Griffiths, M., Yao, S.Y.M., Abidi, F., Phillips, S.E.V., Cass, C.E., Young, J.D., Baldwin, S.A. (1997). Molecular Cloning and Characterization of nitrobenzylthioinosine-insensitive (ei) equilibrative nucleoside transporter from human placenta. Biochem J. 328: 739-743.

48. Griffiths, M., Beaumont, N., Yao, S.Y.M., Sundaram, M., Boumah, C.E., Davies, A., Kwong, F.Y.P., Coe, I., Cass, C.E., Young, J.D., Baldwin, A. (1997). Cloning of a human nucleoside transporter implicated in the cellular uptake of adenosine and chemotherapeutic drugs. Nat Med. 3(1): 89-93.

49. Griswold, I.J., Dahlquist, F.W. (2002). Bigger is better : megadalton protein NMR in solution. Nat Struct Biol. 9(8): 567-568.

50. Haberman, Y., Grimberg, E., Fukuda, M., Sagi-Einsenberg, R. (2003). Synaptotagmin IX, a possible linker between the perniculear and endocytic recycling compartment and the microtubules. J Cell Sci. 116(Pt 21): 4307-4318.

51. Handa, M., Choi, D. S., Caldeiro, R. M., Messing, R. O., Gordon, A.S., Diamond, I. (2001). Cloning of a novel isoform of the mouse NBMPR-sensitive equilibrative nucleoside transporter (ENT1) lacking a putative phosphorylation site. Gene. 262: 301-317.

52. Hyde, R.J., Cass, C.E., Young, J,D., Baldwin, S. A. (2001). The ENT family of eukaryote nucleoside and nucleobase transporters : recent advances in the investigation of structure / function relationships and the identification of novel isoforms. Mol Membr Biol. 18: 53-63.

53. Igumenova, T.I., Frederick, K.K., Wand, A.J. (2006). Characterization of the fast dynamics of protein amino acid side chains using NMR relaxation in solution. Chem Rev. 106(5), 1672-99.

54. Ikura, M., Clore, G.M., Gronenborn, A.M., Zhu, G., Klee, C.B., Bax, A. (1992). Solution structure of a calmodulin-target peptide complex by multidimensional NMR. Science. 256(5057):632-8.

55. Ishima, R., Torchia, D.A. (2000). Protein dynamics from NMR. Nat Struct Biol. 7(9): 740-3.

56. Iwamoto, N., Lu, R., Tanaka, N., Abe-Dohmae, S., Yokoyama, S. (2010). Calmodulin interacts with ATP binding cassette transporter A1 to protect from calpain-mediated degradation and upregulates high-density lipoprotein generation. Arterioscler Thromb Vasc Biol. 30(7): 1446-52.

57. Iyer, K., Bürkle, L., Auerbach, D., Thaminy, S., Dinkel, M., Engels, K., Stagljar, I. (2005). Utilizing the split-ubiquitin membrane yeast two-hybrid system to identify protein-protein interactions of integral membrane proteins. Sci STKE. 275: pl3.

58. Jayanthi, L.D., Annamalai, B., Samuvel D.J., Gether, U., Ramamoorthy, S. (2006). Phosphorylation of the norepinephrine transporter at threonine 258 and Serine 259 is linked to protein kinase C-mediated transporter internalization. J Biol Chem. 281(33): 23326-23340.

59. Jessard, P., Attard, J.J., Carpenter, T.A., Hall, L.D. (1991). Nuclear Magnetic Resonance Imaging in the Solid State. Progress in NMR spectroscopy. 23: 1-41.

60. Johnsson, N., and Varshavsky, A. (1994). Split ubiquitin as a sensor of protein interactions in vivo. Proc Natl Acad Sci. 91: 10340-10344.

61. Jones, S., and Thornton, J.M. (1996). Principles of protein-protein interactions. Proc Natl Acad Sci. 93: 13-20.

62. Kahn, C.R. and White, M.F. (1988). The insulin receptor and the molecular mechanism of insulin action. J Clin Invest. 82: 1151-1156.

63. Kerppola, T.K. (2006). Design and implementation of bimolecular fluorescence complementation (BiFC) assays for the visualization of protein interactions in living cells. Nat Protoc. 1(3): 1278-1286.

64. King, A. E., Ackley, M. a, Cass, Carol E, Young, James D, & Baldwin, Stephen a. (2006). Nucleoside transporters: from scavengers to novel therapeutic targets. Trends Pharmacol Sci. 27(8): 416-25.

65. Kittanakom. S., Chuk. M., Wong. V., Snyder. J., Edmonds. D., Lydakis. A., Zhang. Z., Auerbach. D., Stagljar. I. (2009). Analysis of membrane protein complexes using the split-ubiquitin membrane yeast two-hybrid (MYTH) system. Methods Mol Biol. 548: 247-271.

66. Knight, D., Harvey, P.J., Iliadi, K.G., Klose, M.K., Iliadi, N., Dolezelova, E., Charlton, M.P., Zurovec, M., Boulianne, G.L. (2010). Equilibrative nucleoside

transporter 2 regulates associative learning and synaptic function in Drosophila. J Neurosci. 30(14): 5047-5057.

67. Knuefermann P, Chen P, Misra A, Shi SP, Abdellatif M, Sivasubramanian N. (2002). Myotrophin/V-1, a Protein up-regulated in the failing human heart and in postnatal cerebellum, converts NF B p50-p65 heterodimers to p50-p50 and p65-p65 homodimers. J Biol Chem. 277 (26): 23888–23897

68. Lai, Y., Tse, C.M., Unadkat, J. D. (2004). Mitochondrial expression of the human equilibrative nucleoside transporter 1 (hENT1) results in enhanced mitochondrial toxicity of antiviral drugs. J Biol Chem. 279(6): 4490-7.

69. LeTilly, V., and Royer, C.A. (1993). Fluorescence anisotropy assays implicate protein-protein interactions in regulating trp repressor DNA binding. Biochemistry. 32(30): 7753-8.

70. Lee, E.W., Lai, Y., Zhang, H., & Unadkat, J. D. (2006). Identification of the mitochondrial targeting signal of the human equilibrative nucleoside transporter 1 (hENT1): implications for interspecies differences in mitochondrial toxicity of fialuridine. J Biol Chem. 281(24): 16700-6.

71. Lin, T., Tang, N., Ostap, E.M. (2005). Biochemical and motile properties of Myo1b splice isoforms. J Biol Chem. 280(50): 41562-41567.

72. Longley, D.B., Harkin, D.P., Johnston, P.G. (2003). 5-Fluorouracil: Mechanisms of Action and Clinical Strategies. Nature. 3: 330-338.

73. Mangravite, L. M., Xiao, G., & Giacomini, K. M. (2003). Localization of human equilibrative nucleoside transporters, hENT1 and hENT2, in renal epithelial cells. Am J Physiol Renal Physiol. 284(5): F902-10.

74. Michalet, X., Ekong, R., Fougerousse, F., Rousseaux, S., Schurra, C., Hornigold, N., Slegtenhorst, M.V., Wolfe, J., Povey, S., Beckmann, J.S., Bensimon, A. Dynamic molecular combing: stretching the whole human genome for high-resolution studies. (1997). Science. 277: 1518-1523.

75. Minton, A.P. (2001). The influence of macromolecular crowding and macromolecular confinement on biochemical reactions in physiological media. J Biol Chem. 276(14): 10577-10580.

76. Miwa, N., Kurosaki, K., Yoshida, Y., Kurokawa, M. (2005). Comparative efficacy of acyclovir and vidarabine on the replication of varicella-zoster virus. Antiviral Res. 65: 49-55.

77. Molina-Arcas, M., Trigueros-Motos, L., Casado, F. J., & Pastor-Anglada, M. (2008). Physiological and pharmacological roles of nucleoside transporter proteins. Nucleosides Nucleotides Nucleic acids. 27(6): 769-78.

78. Ngo, L.Y., Patil, S.D., Unadkat, J.D. (2001). Ontogenic and longitudinal activity of Na^+ -nucleoside transporters in the human intestine. Am J Physiol Gastrointest Liver Physiol. 280: G475-G481.

79. Nguyen, H. And Higuchi, H. (2005). Motility of Myosin V regulated by the dissociation of single calmodulin. Nat Struct Mol Biol. 12(2): 127-132.

80. Nice, E., Catimel, B., Stacker, S., Runting, A., Wilks, A., Nicola, N., Burgess, A. (1997). Strategies for the identification and purification of ligands for orphan biomolecules. Lett Peptide Sci. 4: 107-120.

81. Nivillac, N. M. I., Bacani, J., & Coe, I. R. (2011). The life cycle of human equilibrative nucleoside transporter 1: from ER export to degradation. Exp Cell Res. 317(11): 1567-79.

82. Nooren, I.M.A., and Thornton, J.M. (2003). Diversity of protein - protein interactions. The EMBO Journal. 22(14): 3487-3492.

83. Ogbomo, H., Michaelis, M., Klassert, D., Doerr, H. W., Cinatl, J. (2008). Resistance to cytarabine induces the up-regulation of NKG2D ligands and enhances natural killer cell lysis of leukemic cells. Neoplasia. 10(12): 1402-1410.

84. Pattnaik, P. (2005). Surface Plasmon Resonance: Applications in Understanding Receptor-Ligand Interaction. Applied Biochemistry and Biotechnology. 126: 79-92

85. Pelt, K.V., Haan, G.D., Vellenga, E., Daenen, S.M.G.J. (2005). Administration of low-dose cytarabine results in immediate S-phase arrest and subsequent activation of cell cycling in murine stem cells. Exp Hematol. 33: 226-231.

86. Pennycooke, M., Chaudary, N., Shuralyova, I., Zhang. Y., Coe, I.R. (2001). Differential expression of human nucleoside transporters in normal and tumor tissue. Biochem Biophys Res Commun. 280(3): 951-959.

87. Puig, O., Caspary, F., Rigaut, G., Rutz, B., Bouveret, E., Bragado-nilsson, E., Wilm, M. (2001). The tandem affinity Purification (TAP) method : a general procedure of protein complex purification. Methods. 24: 218-229.

88. Qiu, X.B., Shao, Y.M., Miao, S., Wang, L. (2006). The diversity of the DnaJ/Hsp40 family, the crucial partners for Hsp70 chaperones. Cell Mol Life Sci. 63(22):2560-70.

89. Reyes, G., Nivillac, N.M., Chalsev, M., Coe, I.R. (2011). Analysis of recombinant tagged equilibrative nucleoside transporter 1 (ENT1) expressed in E. coli. Biochem Cell Biol. 89(2):246-55.

90. Reyes, G., Nivillac, N.M., Karim, M.Z., Desouza, L., Siu, K.W., Coe, I.R. (2011). The Equilibrative Nucleoside Transporter (ENT1) can be phosphorylated at multiple sites by PKC and PKA. Mol Membr Biol. 28(6): 412-26

91. Rhoads, A.R., Friedberg, F. (1997). Sequence Motifs for Calmodulin Recognition. The FASEB Journal. 11: 331-340.

92. Rich, T. C. & Karpen, J. W. (2002). Review Article: Cyclic AMP Sensors in Living Cells: What Signals Can They Actually Measure? Annals of Biomedical Engineering, 30(8): 1088-1099.

93. Rigaut, G., Shevchenko, A., Rutz, B., Wilm, M., Mann, M., Séraphin, B. (1999). A generic protein purification method for protein complex characterization and proteome exploration. Nat Biotechnol. 17: 1030-1032.

94. Ritzel, M.W.L., Yao, S.Y.M., Huang, M.Y., Elliott, J.F., Cass. C.E., Young, J.D. (1997). Molecular cloning and functional expression of cDNAs encoding a human Na^+-nucleoside cotransporter (hCNT1). Am J Physiol. 272: C707-14.

95. Ritzel, M.W., Ng, A.M., Yao, S.Y., Graham, K., Loewen, S.K., Smith, K.M., Ritzel, R.G., Mowles, D.A., Carpenter, P., Chem, X.Z., Karpinski, E., Hyde, R.J., Baldwin, S.A., Carol, C.E., Young, J.D. (2001). Molecular identification and characterization of novel human and mouse concentrative Na+-nucleoside cotransporter proteins (hCNT3 and mCNT3) broadly selective for purine and pyrimidine nucleosides (system cib). J Biol Chem. 276(4): 2914-27.

96. Rose, J. B., & Coe, I. R. (2008). Physiology of nucleoside transporters: back to the future. . . . Physiology. 23: 41-8.

97. Rose, J. B., Naydenova, Z., Bang, A., Eguchi, M., Sweeney, G., Choi, D.-S., Hammond, J. R., et al. (2010). Equilibrative nucleoside transporter 1 plays an essential role in cardioprotection. Am J Physiol Heart Circ Physiol. 298(3): H771-H777

98. Saenger, W. (1973). Structure and Function of Nucleosides and Nucleotides. Angew Chem Internat Edit. 12(8): 591- 601.

99. Salazar, C., and Ho, T. (2009). Multisite protein phosphorylation – from molecular mechanisms to kinetic models. FEBS Journal. 276: 3177-3198.

100. Salim, N.N., and Feig, A.L. (2009). Isothermal Titration Calorimetry of RNA. Methods. 47(3): 198-205.

101. Scheeff, E.D., and Bourne, P.E. (2005). Structural evolution of the protein kinase-like superfamily. PLoS Comp Biol. 1(5): e49.

102. SenGupta, D.J., Lum, P.Y., Lai, Y., Shubochkina, E., Bakken, A.H., Schneider, G., Unadkat, J.D. (2002). A single glycine mutation in the equilibrative nucleoside transporter gene, hENT1, alters nucleoside transport activity and sensitivity to nitrobenzylthioinosine. Biochemistry. 41(5): 1512-9.

103. Serebriiskii, I., Estojak, J., Berman, M., and Golemis, E.A. (2000). Approaches to detecting false positives in yeast two-hybrid systems. Biotechniques 28: 328–330, 332–326.

104. Shen, W., Kim, J.-Seung., Kish, P.E., Zhang, J., Mitchell, S., Gentry, B.G., Breitenbach, J.M., Drach, J.C., Hilfinger, J. (2009). Bioorganic & Medicinal Chemistry Letters Design and synthesis of vidarabine prodrugs as antiviral agents. Bioorg Med Chem Lett. 19(3): 792-796.

105. Snider, J., Kittanakom, S., Damjanovic, D., Curak, J., Wong, V., Stagljar, I. (2010). Detecting interactions with membrane proteins using a membrane two-hybrid assay in yeast. Nat Prot. 5(7): 1281-1293.

106. Stagljar, I., C. Korostensky, N. Johnsson, and H. S. te. 1998. A genetic system based on split ubiquitin for the analysis of interactions between membrane proteins in vivo. Proc Natl Acad Sci. 95:5187-5192.

107. Stagljar, I., and Fields, S. (2002). Analysis of membrane protein interactions using yeast-based technologies. Trends in biochemical sciences. 27(11): 559-563.

108. Stock, J. B., Ninfa, A.J., Stock, A.M. (1989). Protein phosphorylation and regulation of adaptive responses in bacteria. Microbiol Rev. 53: 450-90

109. Sundaram, M, Yao, S. Y., Ingram, J. C., Berry, Z.A, Abidi, F, Cass, C.E., Baldwin, S.A., Young, J.D. (2001). Topology of a human equilibrative, nitrobenzylthioinosine (NBMPR)-sensitive nucleoside transporter (hENT1) implicated in the cellular uptake of adenosine and anti-cancer drugs. J Biol Chem. 276(48): 45270-5.

110. Taylor, S.S., Yang, J., Wu, J., Haste, N.M., Radzio-Andzelm, E., Anand, G. (2004). PKA: a portrait of protein kinase dynamics. Biochimica et biophysica acta. 1697: 259-69.

111. Velazquez-Campoy, A., Ohtaka, H., Nezami, A., Muzammil, S., Freire, E. (2004). Isothermal Titration Calorimetry. Curr Prot Cell Biol. 17.8.1–17.8.24.

112. Vaynberg, J., & Qin, J. (2006). Weak protein-protein interactions as probed by NMR spectroscopy. Trends Biotechnol. 24(1): 22-7.

113. Vickers, M.F., Mani, R.S., Sundaram, M., Hogue, D.L., Young, J.D., Baldwin, S.A., Cass, C.E. (1999). Functional production and reconstitution of the human equilibrative nucleoside transporter (hENT1) in Saccharomyces cerevisiae. Interaction of inhibitors of nucleoside transport with recombinant hENT1 and a glycosylation-defective derivative (hENT1/N48Q). Biochem J.339: 21-32.

114. Visser, F., Vickers, M.F., Ng, A.M.L., Baldwin, S.A., Young, J.D., Cass, C.E. (2002). Mutation of residue 33 of human equilibrative nucleoside transporters 1 and 2 alters sensitivity to inhibition of transport by dilazep and dipyridamole. J Biol Chem. 277(1): 395-401.

115. Wang, W-S., Tzeng, C-H., Chiou, T-J., Liu, J-H,, Hsieh, R-K., Yen, C-C., Chen, P-M. (1997). High-dose Cytarabine and Mitoxantrone as Salvage Therapy for Refractory Non-Hodgkin ' s Lymphoma. Jpn J Clin Onc. 27(3): 154-157.

116. Ward, J. L., Leung, G.P.H., Toan, S.V., Tse, C.M. (2003). Functional analysis of site-directed glycosylation mutants of the human equilibrative nucleoside transporter-2. Arch Biochem Biophys. 411(1): 19-26.

117. Watterson, J., Toogood, I., Nieder, M., Morse. M., Frierdich, S., Lee, Y., Moertel, C.L., Priest, J.R. (1994). Excessive Spinal Cord Toxicity from Intensive Central Nervous System- Directed Therapies. Cancer. 74(11): 3034-3041.

118. van Weeren, P.C., de Bruyn, K.M., de Vries-Smits, A.M., van Lint, J., Burgering, B.M. (1998). Essential role for protein kinase B (PKB) in insulin-induced glycogen synthase kinase 3 inactivation. Characterization of dominant-negative mutant of PKB. J Biol Chem. 273(21): 13150-6.

119. Vaughen, R.A., Huff, R.A., Uhl, G.R., Kuhar, M.J. (1997). Protein Kinase C-mediated PHosphorylation and Functional Regulation of Dopamine Transporters in Striatal Synaptosomes. J Biol Chem. 272(24): 15541-6.

120. Welcker, M., Orian, A., Jin, J., Grim, J.E., Harper, J.W., Eisenman, R.N., Clurman, B.E. (2004). The Fbw7 Tumor Suppressor Regulates Glycogen Synthase Kinase 3 Phosphorylation-dependent c-Myc Protein Degradation. Proc Natl Acad Sci. 101(24): 9085-9090.

121. Wüthrich, K. (1990). Protein Structure Determination in Solution by NMR Spectroscopy. J Biol Chem. 265 (36): 22059-22062.

122. Xiao, S.H., Manley, J.L. (1997). Phosphorylation of the ASF/SF2 RS domain affects both protein-protein and protein-RNA interactions and is necessary for splicing. Genes Develop. 11(3): 334-344.

123. Yao, S.Y.M., Ng, A.M.L., Vickers, M.F., Sundaram, M., Cass, C.E, Baldwin, S.A., Young, J.D. (2002). Functional and molecular characterization of nucleobase transport by recombinant human and rat equilibrative nucleoside transporters 1 and 2. Chimeric constructs reveal a role for the ENT2 helix 5-6 region in nucleobase translocation. J Biol Chem. 277(28): 24938-48.

124. Yao, S. Y., Ng, A.M., Muzyka, W. R., Griffiths, M., Cass, C E., Baldwin, S A., & Young, J D. (1997). Molecular cloning and functional characterization of nitrobenzylthioinosine (NBMPR)-sensitive (es) and NBMPR-insensitive (ei) equilibrative nucleoside transporter proteins (rENT1 and rENT2) from rat tissues. J Biol Chem. 272(45): 28423-30.

125. Yap, K.L., Kim, J., Truong, K., Sherman, M., Yuan, T., Ikura, M. (2000). Calmodulin target database. J Sruct Funct Genom. 1(1): 8-14.

126. Zamzow, C.R., Bose, R., Parkinson, F.E. (2009). N-methyl-D-aspartate-evoked adenosine and inosine release from neurons requires extracellular calcium. Can Journal Physiol Pharmacol. 87(10): 850-8.

127. Zhou, Y., Yang, W., Lurtz, M.M., Ye. Y., Huang, Y., Lee, H.W., Chen, Y., Louis, C.F., Yang, J.J. (2007). Identification of the Calmodulin Binding Domain of Connexin43*. J Biol Chem. 282(48): 35005-35017.

128. Zhou, Y., Yang, W., Lurtz, M.M., Chen, Y., Jiang, J., Huang, Y., Louis, C.F., Yang. J.J. (2009). Calmodulin Mediates the Ca^{2+}-Dependent Regulation of Cx44 Gap Junctions. Biophys J. 96: 2832-2848.

Appendix

Table - 2: Raw anisotropy data with averaged normalized data of the three runs with hENT1s CaM binding site at a constant 2uM throughout the runs.

[CaM]uM	Run	G	VV	VH	Anisotropy	relative	normalized
0	1	0.885	252.183	185.438	0.15173866	0	0
2		0.885	282.697	196.23	0.17306235	0.021324	0.189543579
4		0.885	263.092	175.976	0.18684117	0.035103	0.312021758
8		0.885	324.34	201.309	0.21476537	0.063027	0.560236416
16		0.885	321.267	188.032	0.23675669	0.085018	0.755714531
32		0.885	320.807	180.121	0.25233673	0.100598	0.894203503
64		0.885	366.99	201.134	0.26139301	0.109654	0.97470363
75		0.885	404.664	220.368	0.26379045	0.112052	0.996014131
95		0.885	395.02	214.859	0.26423886	0.1125	1
0	2	0.908	252.722	183.767	0.14641079	0.146411	0.554085008
2		0.908	240.251	152.298	0.19729034	0.19729	0.746636365
4		0.908	244.276	154.611	0.19786553	0.197866	0.748813139
8		0.908	298.245	179.764	0.21613584	0.216136	0.817956315
16		0.908	359.305	205.136	0.23644978	0.23645	0.894833504
32		0.908	322.375	178.037	0.24890792	0.248908	0.941980767
64		0.908	452.316	242.175	0.26053087	0.260531	0.985967286
75		0.908	425.387	226.044	0.26336111	0.263361	0.996678196
95		0.908	440.668	234.360	0.26304759	0.263048	0.995491698
0	3	0.885	168.26	122.469	0.15550714	0.155507	0.58850974
2		0.885	274.015	181.623	0.19022835	0.190228	0.719910585
4		0.885	319.2	204.498	0.20291704	0.202917	0.76793037
8		0.885	317.307	194.842	0.21878101	0.218781	0.827966847
16		0.885	343.221	197.361	0.24338535	0.243385	0.921080833
32		0.885	360.735	202.831	0.2517966	0.251797	0.952912849
64		0.885	393.542	211.356	0.26899506	0.268995	1.01799964
75		0.885	417.283	225.093	0.2673487	0.267349	1.011769053
95		0.885	395.287	211.211	0.27091017	0.27091	1.025247272
Averaged	**normalized**	**data**					**0**
							0.308878275
							0.387998528
							0.568772946
							0.763054855
							0.869116949
							0.978843762
							0.989280328
							1

Table - 3: Mascot results for mENT1 tryptic peptide REEpSGVPGPNSPPTNR 1261.6284 m/z, with the phosphosite assigned to the fourth residue.

#	b	b^{++}	b^{*}	b^{*++}	b^{0}	b^{0++}	Seq.	y	y^{++}	y^{*}	y^{*++}	y^{0}	y^{0++}	#
1	157.1084	79.0578	140.0818	70.5446			R							16
2	286.1510	143.5791	269.1244	135.0659	268.1404	134.5738	E	1617.6905	809.3489	1600.6639	800.8356	1599.6799	800.3436	15
3	415.1936	208.1004	398.1670	199.5872	397.1830	199.0951	E	1488.6479	744.8276	1471.6213	736.3143	1470.6373	735.8223	14
4	582.1919	291.5996	565.1654	283.0863	564.1814	282.5943	S	1359.6053	680.3063	1342.5787	671.7930	1341.5947	671.3010	13
5	639.2134	320.1103	622.1868	311.5971	621.2028	311.1051	G	1192.6069	596.8071	1175.5804	588.2938	1174.5963	587.8018	12
6	**738.2818**	369.6445	721.2553	361.1313	720.2712	360.6393	V	1135.5854	568.2964	1118.5589	559.7831	1117.5749	559.2911	11
7	835.3346	418.1709	818.3080	409.6577	817.3240	409.1656	P	***1036.5170***	518.7622	1019.4905	510.2489	1018.5065	509.7569	10
8	**892.3560**	446.6817	875.3295	438.1684	874.3455	437.6764	G	***939.4643***	470.2358	922.4377	461.7225	921.4537	461.2305	9
9	989.4088	495.2080	972.3823	486.6948	971.3982	486.2028	P	***882.4428***	441.7250	865.4163	433.2118	864.4322	432.7198	8
10	**1103.4517**	552.2295	1086.4252	543.7162	1085.4412	543.2242	N	***785.3900***	393.1987	768.3635	384.6854	767.3795	384.1934	7
11	**1190.4838**	595.7455	1173.4572	587.2322	1172.4732	586.7402	S	***671.3471***	336.1772	654.3206	327.6639	653.3365	327.1719	6
12	1287.5365	644.2719	1270.5100	635.7586	1269.5260	635.2666	P	***584.3151***	292.6612	567.2885	284.1479	566.3045	283.6559	5
13	1384.5893	692.7983	1367.5627	684.2850	1366.5787	683.7930	P	***487.2623***	244.1348	470.2358	235.6215	469.2518	235.1295	4
14	1485.6370	743.3221	1468.6104	734.8088	1467.6264	734.3168	T	***390.2096***	195.6084	373.1830	187.0951	372.1990	186.6031	3
15	1599.6799	800.3436	1582.6533	791.8303	1581.6693	791.3383	N	289.1619	145.0846	272.1353	136.5713			2
16							R	***175.1190***	88.0631	158.0924	79.5498			1

Table - 4: Mascot results for hENT1 tryptic peptide EEpSGVSVSNSQPTNESHSIK at 2194.94 m/z, with the phosphosite assigned to the third residue.

#	a	a^{++}	a^{*}	a^{*++}	b	b^{++}	b^{*}	b^{*++}	Seq.	y	y^{++}	y^{*}	y^{*++}	#
1	102.0550	51.5311			130.0499	65.5286			E					20
2	231.0975	116.0524			259.0925	130.0499			E	1968.9257	984.9665	1951.8992	976.4532	19
3	300.1190	150.5631			328.1139	164.5606			S	1839.8831	920.4452	1822.8566	911.9319	18
4	357.1405	179.0739			**385.1354**	193.0713			G	1770.8617	885.9345	1753.8351	877.4212	17
5	456.2089	228.6081			**484.2038**	242.6055			V	1713.8402	857.4237	1696.8137	848.9105	16
6	543.2409	272.1241			**571.2358**	286.1216			S	1614.7718	807.8895	1597.7453	799.3763	15
7	642.3093	**321.6583**			**670.3042**	335.6558			V	1527.7398	764.3735	1510.7132	755.8603	14
8	729.3414	365.1743			757.3363	379.1718			S	1428.6714	714.8393	1411.6448	706.3260	13
9	843.3843	422.1958	826.3577	413.6825	871.3792	436.1932	854.3527	427.6800	N	1341.6393	671.3233	1324.6128	662.8100	12
10	930.4163	**465.7118**	913.3898	457.1985	958.4112	479.7093	941.3847	471.1960	S	***1227.5964***	614.3018	1210.5699	605.7886	11
11	1058.4749	529.7411	1041.4483	521.2278	1086.4698	543.7385	1069.4433	535.2253	Q	1140.5644	570.7858	1123.5378	562.2726	10
12	1155.5277	578.2675	1138.5011	569.7542	1183.5226	592.2649	1166.4960	583.7516	P	***1012.5058***	506.7565	995.4793	498.2433	9
13	1256.5753	628.7913	1239.5488	620.2780	1284.5702	642.7888	1267.5437	634.2755	T	***915.4530***	458.2302	898.4265	449.7169	8
14	1370.6183	685.8128	1353.5917	677.2995	1398.6132	**699.8102**	1381.5866	691.2970	N	***814.4054***	407.7063	797.3788	399.1930	7
15	1499.6609	750.3341	1482.6343	741.8208	1527.6558	764.3315	1510.6292	755.8182	E	***700.3624***	350.6849	683.3359	342.1716	6
16	1586.6929	793.8501	1569.6663	785.3368	1614.6878	807.8475	1597.6612	799.3343	S	***571.3198***	286.1636	554.2933	277.6503	5
17	1723.7518	862.3795	1706.7252	853.8663	1751.7467	876.3770	1734.7202	867.8637	H	***484.2878***	242.6475	467.2613	234.1343	4
18	1810.7838	905.8955	1793.7573	897.3823	1838.7787	**919.8930**	1821.7522	911.3797	S	347.2289	174.1181	330.2023	165.6048	3
19	1923.8679	962.4376	1906.8413	953.9243	1951.8628	976.4350	1934.8363	967.9218	I	260.1969	130.6021	243.1703	122.0888	2
20									K	147.1128	74.0600	130.0863	65.5468	1

Table - 5: Mascot results for hENT1 tryptic peptide AGKEESGVpSVSNSQPTNESHSIK at 2451.09 m/z, with the phosphosite assigned to the ninth residue.

#	a	a^{++}	a^*	a^{*++}	b	b^{++}	b^*	b^{*++}	Seq.	y	y^{++}	y^*	y^{*++}	#
1	44.0495	22.5284			72.0444	36.5258			A					23
2	101.0709	51.0391			***129.0659***	65.0366			G	2381.0617	1191.0345	2364.0351	1182.5212	22
3	229.1659	115.0866	212.1394	106.5733	***257.1608***	129.0840	240.1343	120.5708	K	2324.0402	1162.5237	2307.0136	1154.0105	21
4	358.2085	179.6079	341.1819	171.0946	***386.2034***	193.6053	369.1769	185.0921	E	2195.9452	1098.4763	2178.9187	1089.9630	20
5	487.2511	244.1292	470.2245	235.6159	***515.2460***	258.1266	498.2195	249.6134	E	2066.9026	1033.9550	2049.8761	1025.4417	19
6	574.2831	287.6452	557.2566	279.1319	***602.2780***	301.6427	585.2515	293.1294	S	1937.8600	969.4337	1920.8335	960.9204	18
7	631.3046	316.1559	614.2780	307.6427	***659.2995***	330.1534	642.2729	321.6401	G	1850.8280	925.9176	1833.8015	917.4044	17
8	730.3730	365.6901	713.3464	357.1769	***758.3679***	379.6876	741.3414	371.1743	V	1793.8065	897.4069	1776.7800	888.8936	16
9	897.3714	449.1893	880.3448	440.6760	925.3663	463.1868	908.3397	454.6735	S	1694.7381	847.8727	1677.7116	839.3594	15
10	996.4398	498.7235	979.4132	490.2102	***1024.4347***	512.7210	1007.4081	504.2077	V	1527.7398	764.3735	1510.7132	755.8603	14
11	1083.4718	542.2395	1066.4452	533.7263	1111.4667	556.2370	1094.4402	547.7237	S	***1428.6714***	714.8393	1411.6448	706.3260	13
12	1197.5147	599.2610	1180.4882	590.7477	***1225.5096***	613.2585	1208.4831	604.7452	N	***1341.6393***	671.3233	1324.6128	662.8100	12
13	1284.5467	642.7770	1267.5202	634.2637	1312.5417	656.7745	1295.5151	648.2612	S	***1227.5964***	614.3018	1210.5699	605.7886	11
14	1412.6053	706.8063	1395.5788	698.2930	***1440.6002***	720.8038	1423.5737	712.2905	Q	***1140.5644***	570.7858	1123.5378	562.2726	10
15	1509.6581	755.3327	1492.6315	746.8194	1537.6530	769.3301	1520.6265	760.8169	P	***1012.5058***	506.7565	995.4793	498.2433	9
16	1610.7058	805.8565	1593.6792	797.3432	1638.7007	819.8540	1621.6741	811.3407	T	***915.4530***	458.2302	898.4265	449.7169	8
17	1724.7487	862.8780	1707.7221	854.3647	1752.7436	876.8754	1735.7171	868.3622	N	***814.4054***	407.7063	797.3788	399.1930	7
18	1853.7913	927.3993	1836.7647	918.8860	1881.7862	941.3967	1864.7597	932.8835	E	***700.3624***	350.6849	683.3359	342.1716	6
19	1940.8233	970.9153	1923.7968	962.4020	1968.8182	984.9128	1951.7917	976.3995	S	***571.3198***	286.1636	554.2933	277.6503	5
20	2077.8822	1039.4448	2060.8557	1030.9315	2105.8771	1053.4422	2088.8506	1044.9289	H	***484.2878***	242.6475	467.2613	234.1343	4
21	2164.9143	1082.9608	2147.8877	1074.4475	2192.9092	1096.9582	2175.8826	1088.4450	S	***347.2289***	174.1181	330.2023	165.6048	3
22	2277.9983	1139.5028	2260.9718	1130.9895	2305.9932	1153.5003	2288.9667	1144.9870	I	***260.1969***	130.6021	243.1703	122.0888	2
23									K	***147.1128***	74.0600	130.0863	65.5468	1

Table - 6: Mascot results for hENT1 tryptic peptide EESGVSVpSNSQPTNESHSIK at 2194.94 m/z, with the phosphosite assigned to the eighth residue.

#	a	a^{++}	a^{*}	a^{*++}	b	b^{++}	b^{*}	b^{*++}	Seq.	y	y^{++}	y^{*}	y^{*++}	#
1	102.0550	51.5311			130.0499	65.5286			E					20
2	231.0975	116.0524			259.0925	130.0499			E	1968.9257	984.9665	1951.8992	976.4532	19
3	318.1296	159.5684			346.1245	173.5659			S	1839.8831	920.4452	1822.8566	911.9319	18
4	375.1510	188.0792			403.1460	**202.0766**			G	1752.8511	876.9292	1735.8246	868.4159	17
5	474.2195	237.6134			502.2144	251.6108			V	1695.8297	848.4185	1678.8031	839.9052	16
6	561.2515	281.1294			589.2464	295.1268			S	1596.7612	798.8843	1579.7347	790.3710	15
7	660.3199	330.6636			688.3148	344.6610			V	1509.7292	755.3682	1492.7027	746.8550	14
8	729.3414	365.1743			757.3363	379.1718			S	***1410.6608***	705.8340	1393.6342	697.3208	13
9	843.3843	422.1958	826.3577	413.6825	871.3792	436.1932	854.3527	427.6800	N	1341.6393	671.3233	1324.6128	662.8100	12
10	930.4163	465.7118	913.3898	457.1985	958.4112	479.7093	941.3847	471.1960	S	***1227.5964***	614.3018	1210.5699	605.7886	11
11	1058.4749	529.7411	1041.4483	521.2278	1086.4698	543.7385	1069.4433	535.2253	Q	***1140.5644***	570.7858	1123.5378	562.2726	10
12	1155.5277	578.2675	1138.5011	569.7542	1183.5226	592.2649	1166.4960	583.7516	P	***1012.5058***	506.7565	995.4793	498.2433	9
13	1256.5753	628.7913	1239.5488	620.2780	1284.5702	642.7888	1267.5437	634.2755	T	***915.4530***	458.2302	898.4265	449.7169	8
14	1370.6183	685.8128	1353.5917	677.2995	1398.6132	699.8102	1381.5866	691.2970	N	***814.4054***	407.7063	797.3788	399.1930	7
15	1499.6609	750.3341	1482.6343	741.8208	1527.6558	**764.3315**	1510.6292	755.8182	E	***700.3624***	350.6849	683.3359	342.1716	6
16	1586.6929	793.8501	1569.6663	785.3368	1614.6878	807.8475	1597.6612	799.3343	S	***571.3198***	286.1636	554.2933	277.6503	5
17	1723.7518	862.3795	1706.7252	853.8663	1751.7467	876.3770	1734.7202	867.8637	H	***484.2878***	242.6475	467.2613	234.1343	4
18	1810.7838	905.8955	1793.7573	897.3823	1838.7787	**919.8930**	1821.7522	911.3797	S	***347.2289***	174.1181	330.2023	165.6048	3
19	1923.8679	962.4376	1906.8413	953.9243	1951.8628	**976.4350**	1934.8363	967.9218	I	260.1969	130.6021	243.1703	122.0888	2
20									K	***147.1128***	74.0600	130.0863	65.5468	1